UNCLASSIFIED

SECURITY CLASSIFICATION OF THIS PAGE *(When Data Entered)*

REPORT DOCUMENTATION PAGE

READ INSTRUCTIONS BEFORE COMPLETING FORM

1. REPORT NUMBER: NAVENVPREDRSCHFAC Contractor Report CR 83-01 (a)
2. GOVT ACCESSION NO.:
3. RECIPIENT'S CATALOG NUMBER:

4. TITLE *(and Subtitle)*: Satellite Moisture Retrieval Techniques
Volume 1: Technique Development and Evaluation

5. TYPE OF REPORT & PERIOD COVERED: Final

6. PERFORMING ORG. REPORT NUMBER:

7. AUTHOR(s): A. Rosenberg, D.B. Hogan, C.K. Bowman

8. CONTRACT OR GRANT NUMBER(s): N00228-81-C-H156

9. PERFORMING ORGANIZATION NAME AND ADDRESS:
RCA Government Systems Division
Astro-Electronics
Princeton, NJ 08540

10. PROGRAM ELEMENT, PROJECT, TASK AREA & WORK UNIT NUMBERS:
PE 62759N PN SF59-553
NEPRF WU 6.2-13

11. CONTROLLING OFFICE NAME AND ADDRESS:
Naval Air Systems Command
Department of the Navy
Washington, DC 20361

12. REPORT DATE: January 1983

13. NUMBER OF PAGES: 96

14. MONITORING AGENCY NAME & ADDRESS *(if different from Controlling Office)*:
Naval Environmental Prediction Research Facility
Monterey, CA 93940

15. SECURITY CLASS. *(of this report)*: UNCLASSIFIED

15a. DECLASSIFICATION/DOWNGRADING SCHEDULE:

16. DISTRIBUTION STATEMENT *(of this Report)*:
Approved for public release; distribution unlimited

17. DISTRIBUTION STATEMENT *(of the abstract entered in Block 20, if different from Report)*:

18. SUPPLEMENTARY NOTES:
See also Satellite Moisture Retrieval Techniques VOLUME 2: Atmospheric Sounding Bibliography -- NAVENVPREDRSCHFAC CR 83-01(b) -- for listings developed by literature search in the subject area.

19. KEY WORDS *(Continue on reverse side if necessary and identify by block number)*:
Satellite meteorology
Radiative transfer
Water vapor retrieval
Remote sensing

20. ABSTRACT *(Continue on reverse side if necessary and identify by block number)*:
The water vapor channels of the Special Sensor H-2 (SSH/2) of the Defense Meteorological Satellite Program (DMSP) are analyzed, and their ability to retrieve vertical profiles of moisture is studied.

The sensitivity in the measured radiance for each channel to changes in water vapor amount made at levels throughout the troposphere is calculated. It is determined that the ability of the SSH/2, and indeed of any infrared sensor, to estimate the water vapor at levels near the surface is severely limited.

((continued on reverse))

DD FORM 1 JAN 73 1473 EDITION OF 1 NOV 65 IS OBSOLETE
S/N 0102-014-6601

UNCLASSIFIED

SECURITY CLASSIFICATION OF THIS PAGE *(When Data Entered)*

Block 20, Abstract, continued.

A statistical retrieval technique that relies on correlations of atmospheric humidity with the observed SSH/2 radiances and estimates of the tropospheric temperatures is used to provide a first guess estimate of the moisture profile. This first guess profile is then corrected using a physical approach that inverts the radiative transfer equation. For a sample set of mid-latitude profiles this statistical-physical technique yields fraction root mean squared errors of about 25% for the region 400-700 mb, with errors of about 35% for regions nearer the surface.

ROUTINE REPLY, ENDORSEMENT, TRANSMITTAL OR INFORMATION SHEET

OPNAV 5216/158 (Rev. 7-78) *A WINDOW ENVELOPE MAY BE USED*
SN 0107 LF 052 1691 *Formerly NAVEXOS 3789*

CLASSIFICATION (*UNCLASSIFIED when detached from enclosures, unless otherwise indicated*): UNCLASSIFIED

FROM (*Show telephone number in addition to address*):
Commanding Officer, Naval Environmental Prediction Research Facility, Monterey, CA 93940 AVN 878-2928

DATE: 15 March 1983

SUBJECT:
NAVENVPREDRSCHFAC technical publication; forwarding of

SERIAL OR FILE NO.:
NAVENVPREDRSCHFAC/SBB:sb
5600 SER: 102

TO:

Distribution
[See pp Dist-1--3, Encl (1),(2)]

REFERENCE

ENCLOSURE
(1) NAVENVPREDRSCHFAC Contractor Report CR 83-01 (a): Satellite Moisture Retrieval Techniques, Vol 1, Technique Development and Evaluation
(2) CR 83-01 (b): Vol 2, Atmospheric Sounding Bibliography

VIA:

ENDORSEMENT ON

XX FORWARDED ☐ RETURNED ☐ FOLLOW-UP, OR TRACER ☐ REQUEST ☐ SUBMIT ☐ CERTIFY ☐ MAIL ☐ FILE

GENERAL ADMINISTRATION	CONTRACT ADMINISTRATION	PERSONNEL
FOR APPROPRIATE ACTION	NAME & LOCATION OF SUPPLIER OF SUBJECT ITEMS	REPORTED TO THIS COMMAND:
UNDER YOUR COGNIZANCE	SUBCONTRACT NO. OF SUBJECT ITEM	
XX INFORMATION & retention	APPROPRIATION SYMBOL, SUBHEAD, AND CHARGEABLE ACTIVITY	DETACHED FROM THIS COMMAND
APPROVAL RECOMMENDED ☐ YES ☐ NO	SHIPPING AT GOVERNMENT EXPENSE ☐ YES ☐ NO	OTHER
☐ APPROVED ☐ DISAPPROVED	A CERTIFICATE, VICE BILL OF LADING	
COMMENT AND/OR CONCURRENCE	COPIES OF CHANGE ORDERS, AMENDMENT OR MODIFICATION	
CONCUR	CHANGE NOTICE TO SUPPLIER	
LOANED, RETURN BY:	STATUS OF MATERIAL ON PURCHASE DOCUMENT	
SIGN RECEIPT & RETURN		
REPLY TO THE ABOVE BY:		
REFERENCE NOT RECEIVED		
SUBJECT DOCUMENT FORWARDED TO:		
SUBJECT DOCUMENT RETURNED FOR:		
SUBJECT DOCUMENT HAS BEEN REQUESTED, AND WILL BE FORWARDED WHEN RECEIVED		
COPY OF THIS CORRESPONDENCE WITH YOUR REPLY		
ENCLOSURE NOT RECEIVED		
ENCLOSURE FORWARDED AS REQUESTED		
ENCLOSURE RETURNED FOR CORRECTION AS INDICATED		
CORRECTED ENCLOSURE AS REQUESTED		
REMOVE FROM DISTRIBUTION LIST		
REDUCE DISTRIBUTION AMOUNT TO:		

REMARKS (*Continue on reverse*)

Enclosure (1) documents a sensitivity study of the DMSP SSH/2 water vapor channels. Enclosure (2) is a bibliography of the field of remote sensing of atmospheric temperature and water vapor.

SIGNATURE & TITLE: Kenneth L. Vonder Haar
Commanding Officer

COPY TO:

CLASSIFICATION (*UNCLASSIFIED when detached from enclosures, unless otherwise indicated*): UNCLASSIFIED

★ G.P.O.: 1979-689-016/4281

NAVENVPREDRSCHFAC
CONTRACTOR REPORT
CR 83-01 (a)

NAVENVPREDRSCHFAC CR 83-01 (a)

SATELLITE MOISTURE RETRIEVAL TECHNIQUES
VOLUME 1
TECHNIQUE DEVELOPMENT AND EVALUATION

Prepared By:

A. Rosenberg, D. B. Hogan, and C. K. Bowman
RCA Government Systems Division,
Astro-Electronics, Princeton, New Jersey 08540

Contract No. N00228-81-C-H156

JANUARY 1983

Prepared For:
NAVAL ENVIRONMENTAL PREDICTION RESEARCH FACILITY,
MONTEREY, CALIFORNIA 93940

TABLE OF CONTENTS

TABLE OF CONTENTS (CONTINUED)

TABLE OF CONTENTS (CONTINUED)

Acknowledgements

The authors wish to give special thanks to M. T. Chahine for his many valuable contributions made throughout this study. We thank T. J. Kleespies for his helpful comments and careful review of this manuscript, and R. D. Haskins who participated in many stimulating discussions. We are also grateful to M. Pfann, who assisted us with her valuable expertise in computer based literature searches.

SECTION 1.0

SUMMARY OF WORK

1.1 INTRODUCTION

Knowledge of the vertical structure of water vapor in the atmosphere is important for many aspects of atmospheric science, ranging from numerical weather forecasting to climate studies to the prediction of severe storms. Satellites provide an ideal platform for monitoring the atmospheric water vapor content because of their global (in the case of polar orbiters) or continuous (in the case of geosynchronous satellites) coverage. Infrared sounders on past, present, and proposed satellites contain water vapor channels from which information on the H_2O content of the atmosphere can be extracted; however, attempts to date to derive accurate H_2O profiles have met with limited success.

This is a report on NEPRF Contract N00228-81-C-H156 "Satellite Moisture Retrieval Techniques" whose purpose is to develop techniques to obtain moisture profiles from satellite observations. This report consists of two volumes. Volume I gives the development of the retrieval technique and its evaluation. Volume II gives a bibliography of papers on satellite moisture and temperature retrievals. Volume I is organized as follows: Section 1 gives a summary of the work. Section 2 describes the data base used for an extensive literature search that is compiled in Volume II. In Section 3 the eight water vapor channels of the SSH/2 sounder are analyzed in detail.

Section 4 outlines our plan to develop the retrieval technique. In Section 5 a statistical retrieval method is developed and its accuracy evaluated. In Section 6 a relaxation-iteration retrieval technique is implemented, using the statistical retrieval as a first guess, and the accuracy of the combined statistical-physical scheme is assessed. The conclusions of the work are drawn in Section 7.

1.2 EXTENSIVE LITERATURE SEARCH

The purpose of the literature search is to determine the state-of-the-art in H_2O soundings and to provide a data base for future research on the subject. Material for the literature search was drawn from two computer data bases as well as the recently published literature. The results of the literature search, which included temperature as well as water vapor sounding techniques, were tabulated and cross referenced. The references were listed in several forms:

- By year of publication (this is the master list)
- By subject
- By satellite instrument

Based on the outcome of the literature search it was decided to investigate the SSH/2 sounder flown onboard the DMSP series of polar orbiting satellites. The SSH/2 is a passive infrared

radiometer with eight H_2O channels. It was selected for two reasons:

- Techniques developed for the SSH/2 to determine water vapor could be adopted for operational use relatively quickly.

- The SSH/2 has the largest number of water vapor channels of any current sounder -- which should allow retrievals from a diverse range of atmospheres.

1.3 WATER VAPOR PROFILES FROM PASSIVE SOUNDERS

Following the literature search, the theory of passive atmospheric constituent retrievals was evaluated with an emphasis on the infrared region. A sensitivity study of the SSH/2 was then performed to determine the response of each H_2O channel to a change in water vapor amount at levels throughout the troposphere. In addition, two types of "weighting functions" were calculated and plotted to aid in selection of possible retrieval methods.

It was concluded that H_2O channels alone do not contain enough information to allow retrievals down to the surface layers. If water vapor at the lowest levels is desired, then either other measurements must be used (e.g., active), or statistical relationships must be derived. A statistical technique, the Smith-Woolf Eigenvalue-Eigenvector Technique[1], was selected to provide a first guess estimate of the tropospheric water vapor structure. It employs as independent variables (1) brightness

temperatures obtained from the H_2O channels and (2) tropospheric temperatures at various levels (which could in practice be determined from CO_2 sounding channels). The water vapor amounts at the different tropospheric levels are the dependent variables.

Due to the high sensitivity of most of the H_2O channels to middle tropospheric water vapor changes, it was felt that the statistically derived profiles could be improved in this region by correcting with a nonlinear relaxation technique based upon inverting the radiative transfer equation. Two relaxation techniques were considered: (1) based on the Chahine[2] method of correcting at selected levels of the atmosphere and interpolating between them using various techniques; and (2) inverting the H_2O channel radiances to obtain a temperature profile in terms of an integrated water vapor amount to that level and mapping to a temperature profile obtained in pressure space[3] (the U-Space Retrieval Technique).

1.4 EVALUATION OF SELECTED RETRIEVAL TECHNIQUE

The Chahine type retrieval method was selected for further development and a simulation study was designed to test it. A set of 1200 profiles of temperature and water vapor was obtained from NOAA/NESS, and divided into three equal groups of 400 profiles from mid-latitude, arctic, and tropical climate regions respectively. Radiances were simulated for each profile for the eight water vapor channels of the SSH/2, using a

rapid transmittance algorithm. This rapid algorithm was generated from "exact" line-by-line calculations and is discussed in Appendix A. Random noise was added to each observation and each climatological group was divided into subsets of dependent and independent profiles. The dependent profiles were used to derive the linear prediction matrix of the Smith-Woolf technique, while the independent set was used to test the accuracy of the statistical first guess, and the improvement offered by the relaxation algorithm.

The results of simulation studies show that the fractional RMS error is about 35% for mid-latitude profiles for the statistical first guess. In the region 400 mb-700-mb the functional RMS error was reduced to about 25% by a relaxation technique.

SECTION 2.0

EXTENSIVE LITERATURE SEARCH

2.1 COMPUTERIZED PUBLICATIONS SEARCH

The computer search was initiated by scanning the Department of Commerce NTIS (National Technical Information Service) Data Base and the INSPEC file of Lockheed's DIALOG Data Base. The NTIS Data Base consists of reports resulting from government contracts and technical reports issued by government agencies. The Lockheed Data Base consists of citations from technical journals. The initial scan was supplemented from personal files.

The Data Bases contained only material published during or after 1967. From examining references in the papers cited, and from information in personal files, it was concluded that very few pre-1967 references were relevant to this study. However, three pre-1967 papers (Kaplan[4], King[3], and Wark and Fleming[5]) were deemed to be important because they formed the basis for most of the satellite retrieval work that followed. The full literature survey is given in Volume II. Section 1 presents the entire bibliography chronologically. Section 2 is classified by subjects and Section 3 is classified by instruments.

The literature search covers the techniques of water vapor retrieval as well as of temperature retrieval, because both techniques employ similar methods and instruments.

The retrieval studies conducted in parallel with the literature search had yielded definite results on the limitations of any single instrument. In particular,

(a) No single instrument discovered has the capability of retrieving water vapor content throughout the atmosphere with high vertical resolution.

(b) A combination of instruments is required to measure H_2O amount at low levels (see Section 3.2). Probably coincident microwave and IR soundings will be necessary.

With the above limitations on the capability of any single instrument, it is possible to conclude from the literature search that the best single sounding instrument for moisture retrievals is the SSH/2.

SECTION 3.0

ANALYSIS OF DMSP-SSH/2 SOUNDER

3.1 DESCRIPTION OF INSTRUMENT AND WEIGHTING FUNCTIONS

The SSH/2 infrared sounder[6] aboard the DMSP satellite contains eight water vapor sounding channels: seven in the 18-28 μm region and one centered at 12.5 μm. Table 3.1 gives the central frequencies and bandwidths of these channels. A plot of the filter response functions $\phi_i(\nu)$ for the H_2O channels (7-14) is given in figure 3.1. The channels are all broadband with a significant degree of overlap in the spectral bandpasses for the 18-28 μm region.

The transmission properties of the atmosphere for the SSH/2 were analyzed using a line-by-line transmission program obtained from the Goddard Laboratory for the Atmospheric Sciences[7] and modified at RCA. The calculations utilize the AFGL Line Compilation tape (1980 version)[8] which includes line parameters for the gases H_2O, CO_2, O_3, N_2O, CO, CH_4 and O_2. Water vapor was the largest contributor to absorption for all SSH/2 channels with smaller amounts of absorption coming from CO_2 and N_2O. The line-by-line program included the effects of induced emission, a significant factor in the 18-28 μm region. The absorption due to the water vapor continuum was not included in the transmission computations.

The absorption was calculated for three atmospheric models[9]: a mid-latitude summer model, a subarctic winter model, and

TABLE 3.1. CENTRAL FREQUENCIES AND BANDWIDTHS FOR THE SSH/2 SOUNDER.

CHANNEL NUMBER (CODE)	WAVELENGTH (μM)	WAVENUMBER (CM^{-1})	HALFWIDTH (CM^{-1})	NESN ① (ERG SEC^{-1} CM^{-1} $STER^{-1}$)	ΔT_B ② (°K)	ABSORPTION (SPECIES)
1(E6)	13.4	747	12.5	.070		LEAST (CO_2)
2(E5)	13.7	731	12.5	.071		↓
3(E4)	14.1	708	12.5	.072		↓
4(E3)	14.4	695	12.5	.067		↓
5(E2)	14.8	676	12.5	.085		↓
6(E1)	15.0	668.5	3.0	.310		MOST (CO_2)
15(E8)	11.1	898	12.5	.054		WINDOW
16(W)	3.7	2700	2425-2900	.0012		WINDOW
7(E7)	12.5	797	12.5	.049	.03	LEAST (H_2O)
8(F1)	18.7	535	15.0	.138	.12	↓
9(F5)	20.1	497	17.0	.120	.12	↓
10(F6)	24.5	408	14.0	.105	.14	↓
11(F4)	22.7	441	20.0	.057	.06	↓
12(F3)	23.9	420	22.0	.087	.11	↓
13(F2)	25.2	397	12.5	.136	.19	↓
14(F8)	28.3	353	14.0	.268	.47	MOST (H_2O)

① Data for Operating Temperature of 25°C.

② Noise Equivalent Brightness Temperature for a Standard Atmosphere

FIGURE 3.1 FILTER RESPONSE FUNCTIONS $\Phi_i(\nu)$ FOR CHANNELS 7-14 OF THE SSH/2 SOUNDER

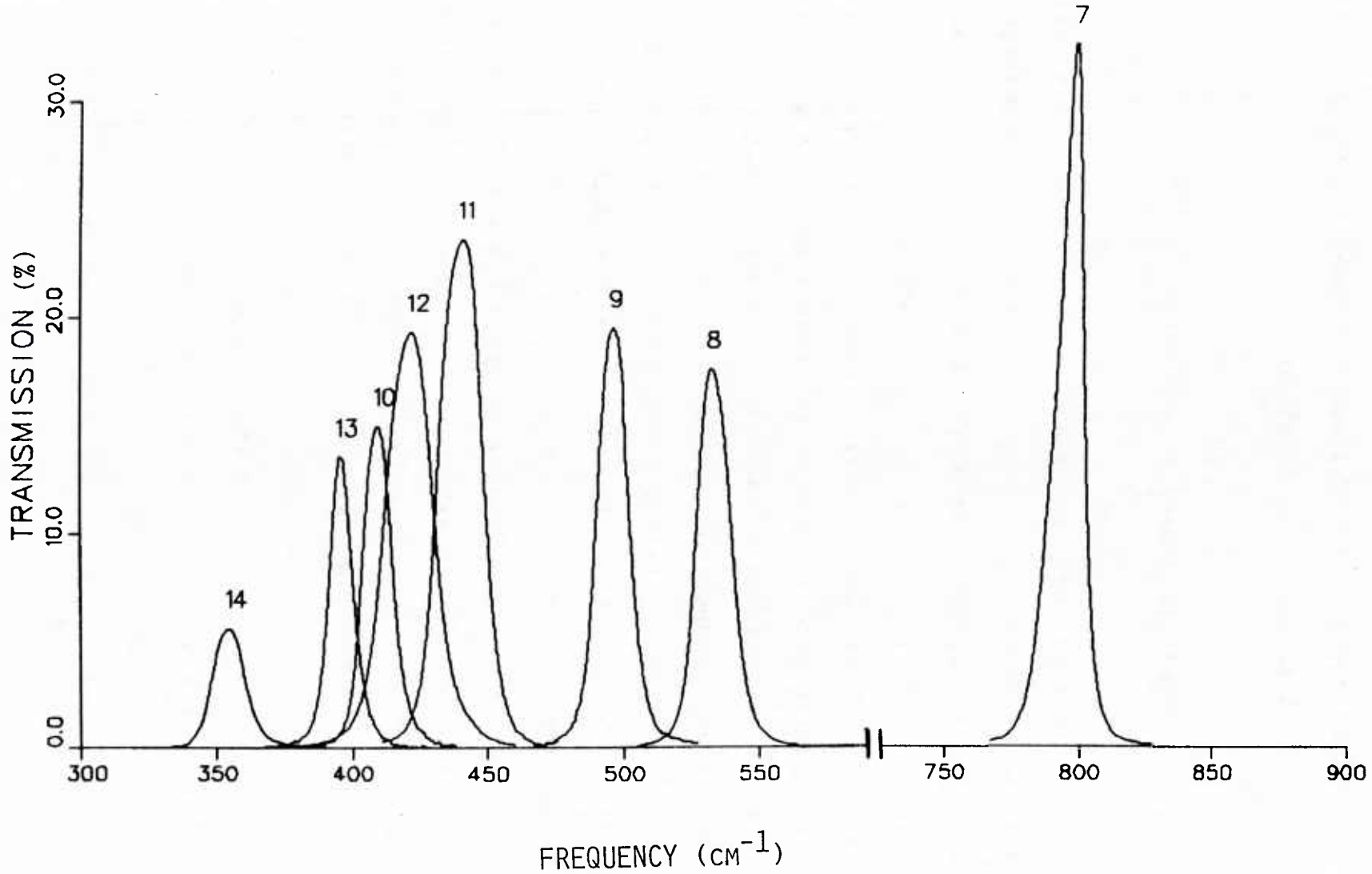

a tropical model. The radiance, r_i, measured by channel i centered at frequency $\bar{\nu}_i$ is given by,

$$r_i = B_{\bar{\nu}i}(T_s)\tau_i(Ps) - \int_o^{Ps} B_{\bar{\nu}i}[T(p)] \frac{\partial \tau_{i(p)}}{\partial \ln p} d\ln p \qquad (1)$$

where p is pressure, p_s the surface pressure, T_s the surface skin temperature, $\tau_i(p)$ the channel averaged transmittance from the top of the atmosphere to pressure p for the atmospheric model in question and $B_{\bar{\nu}_i}(T)$ the Planck emission function at frequency $\bar{\nu}_i$ and temperature T. The derivative $\partial\tau_i/\partial\ln p$ gives the relative contribution of the Planck emission at each level in the atmosphere to the measured radiance. Figures 3.2 - 3.4 show the weighting function $\partial\tau_i/\partial\ln p$ plotted as a function of pressure for the mid-latitude summer, sub-artic winter and tropical models. The weighting functions are distributed throughout the troposphere with channel 7 measuring radiation emitted primarily from the surface and Channel 14 measuring radiation emitted from above 400 mb. Figure 3.5 shows how various atmospheric models affect the weighting functions. A lower tropospheric channel (8) and an upper tropospheric channel (13) were plotted for the three atmospheric models discussed above. Except for some stratospheric levels the amount of water vapor increases as one proceeds from the subarctic winter model through the mid-latitude summer model to the tropical model. This results in the weighting functions peaking nearer the surface for the drier models due to the

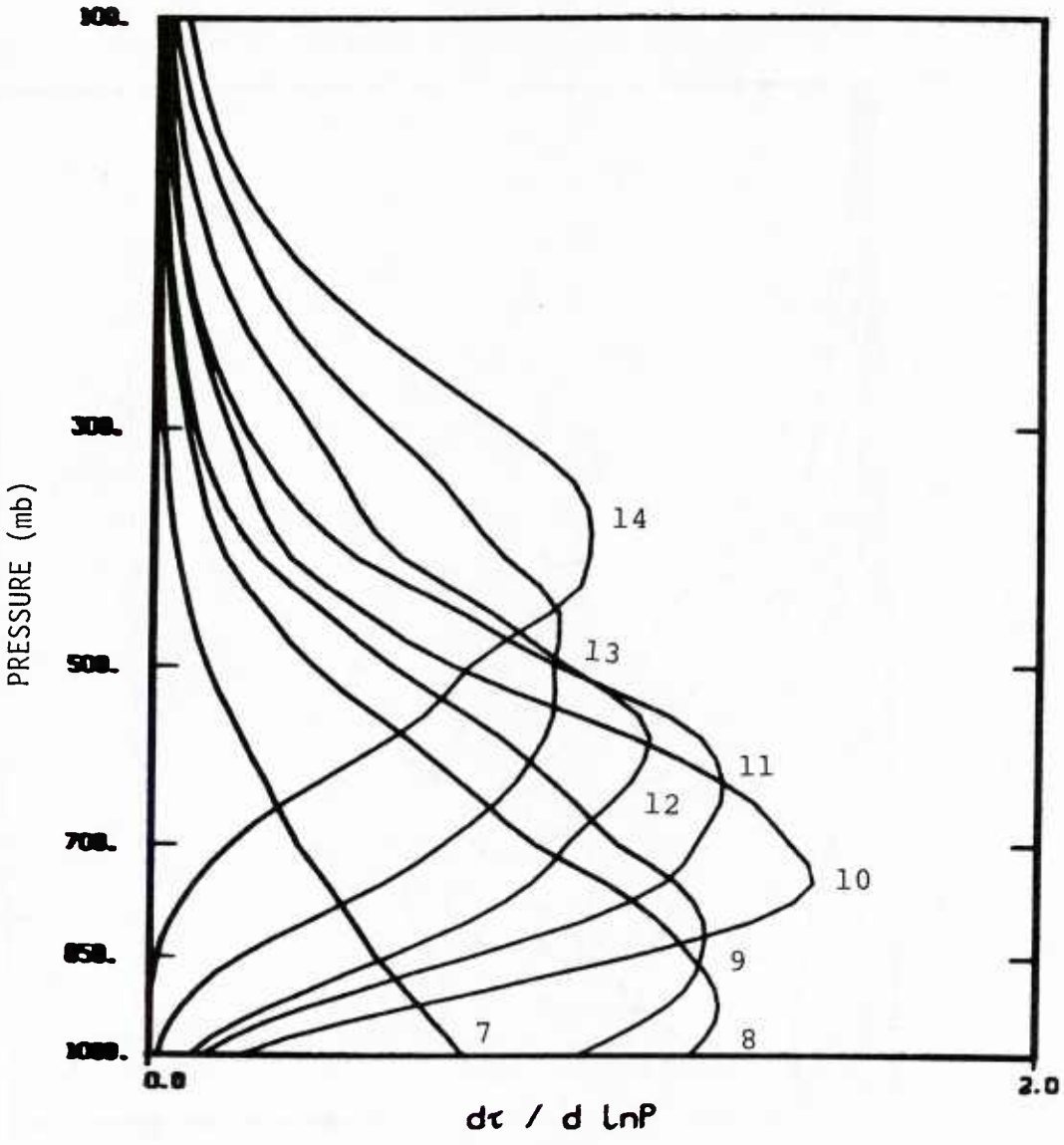

Figure 3.2. Weighting Functions $\partial\tau_i/\partial\ln p$ for Channels 7-14 Of The SSH/2 - Mid-Latitude Summer Profile

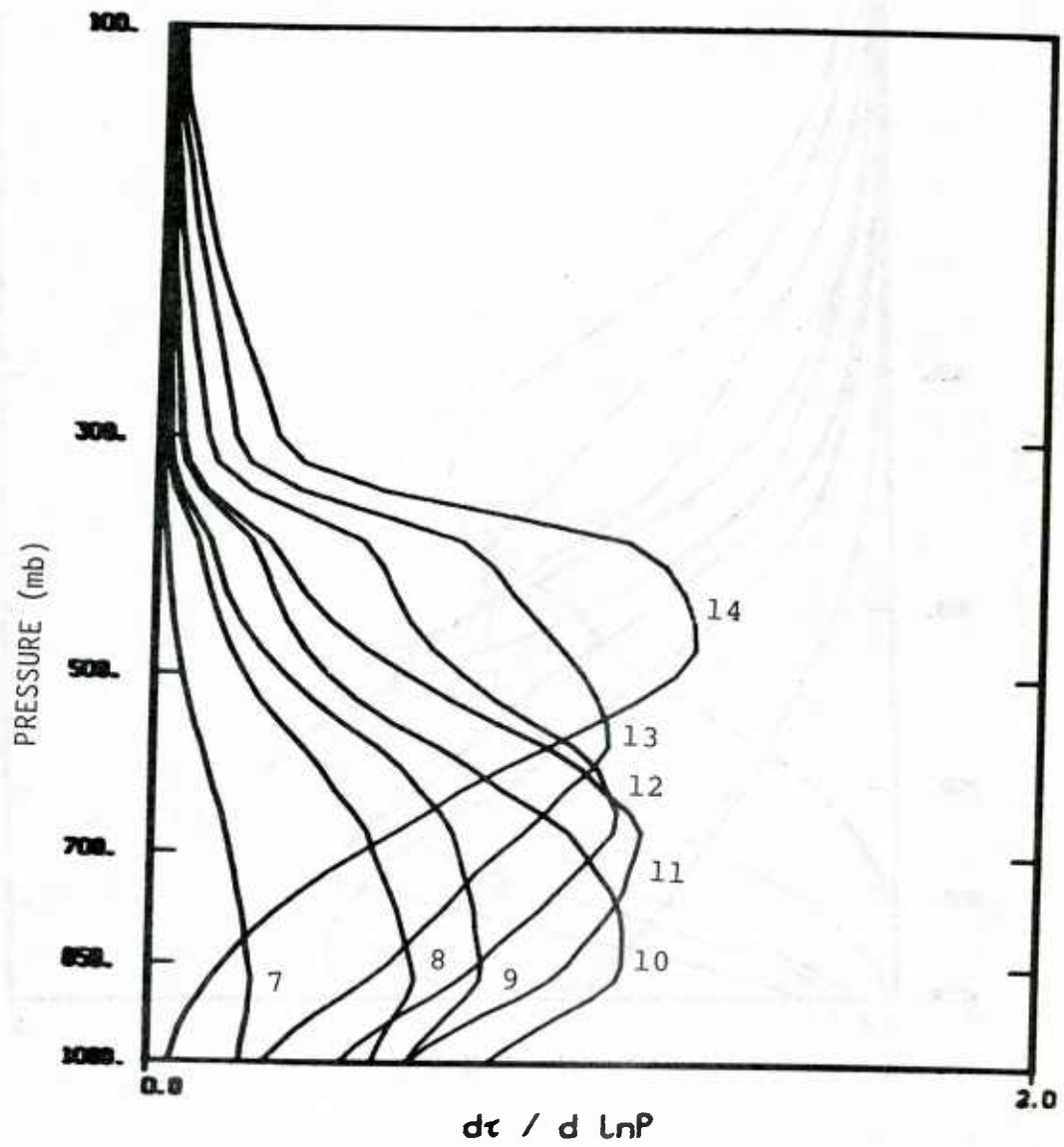

Figure 3.3. Weighting Functions, $\partial\tau_i/\partial\ln p$ for Channels 7-14 of The SSH/2 - Subarctic Winter Profile

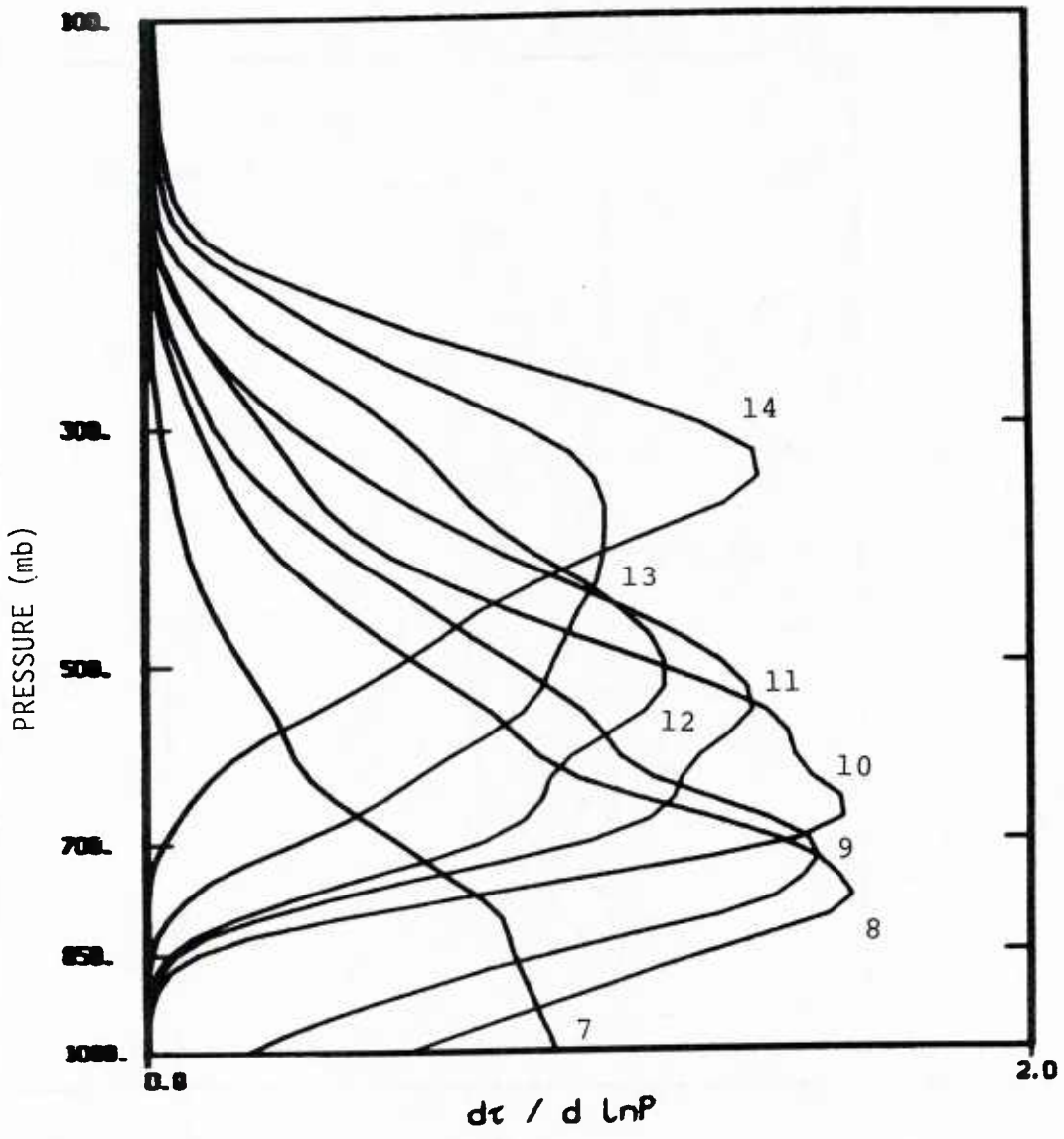

Figure 3.4. Weighting Functions, $\partial\tau_i/\partial\ln p$ for Channels 7-14 of The SSH/2 - Tropical Atmosphere

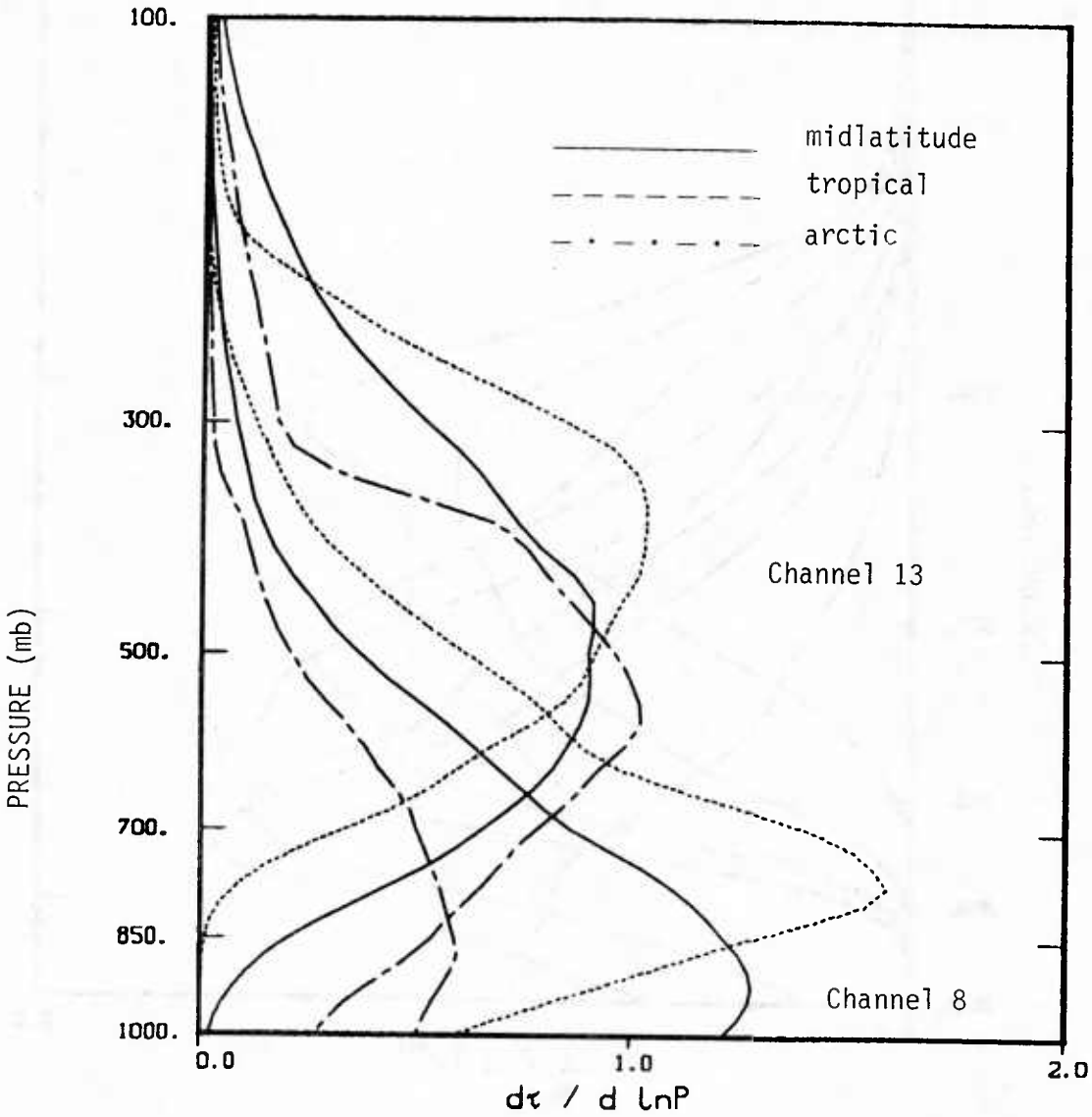

Figure 3.5. Weighting Functions, $\partial\tau_i/\partial\ln p$ for Channels 8 and 13 of The SSH/2 for Three Atmospheric Models

decreased absorption by water vapor. The wetter models peak at higher levels.

This extreme dependence of $\partial\tau_i/\partial\ln p$ upon atmospheric water vapor distribution results in a variation of several hundred millibars in level of peak contribution. This is quite different from temperature sounding channels based upon absorption due to gases of fixed mixing ratio (usually CO_2 for the infrared) where changes in weighting functions are a secondary effect.

Let the integrated water vapor amount from the top of the atmosphere to pressure p to be defined as

$$U(p) = \frac{1}{g}\int_0^P q(p')\, dp' \tag{2}$$

with g the acceleration of gravity and q(p) the mixing ratio of water vapor at pressure p. Now rewrite the radiative transfer equation (R.T.E.), (1), with U(p) as the vertical coordinate

$$r_i = B_{\nu i}(T_s)\tau(U_s) - \int_0^{U_s} B_{\nu i}[T(U)] \frac{\partial\tau}{\partial\ln U} d\ln U \tag{3}$$

where $U_s = U(p_s)$.

Figures 3.6, 3.7 and 3.8 show the weighting functions plotted in this integrated water vapor space or **U**-space. These U-space weighting functions are much less sensitive to atmospheric changes than are the pressure-space functions. Because of the diversity in total water vapor in each of the models, the lowest

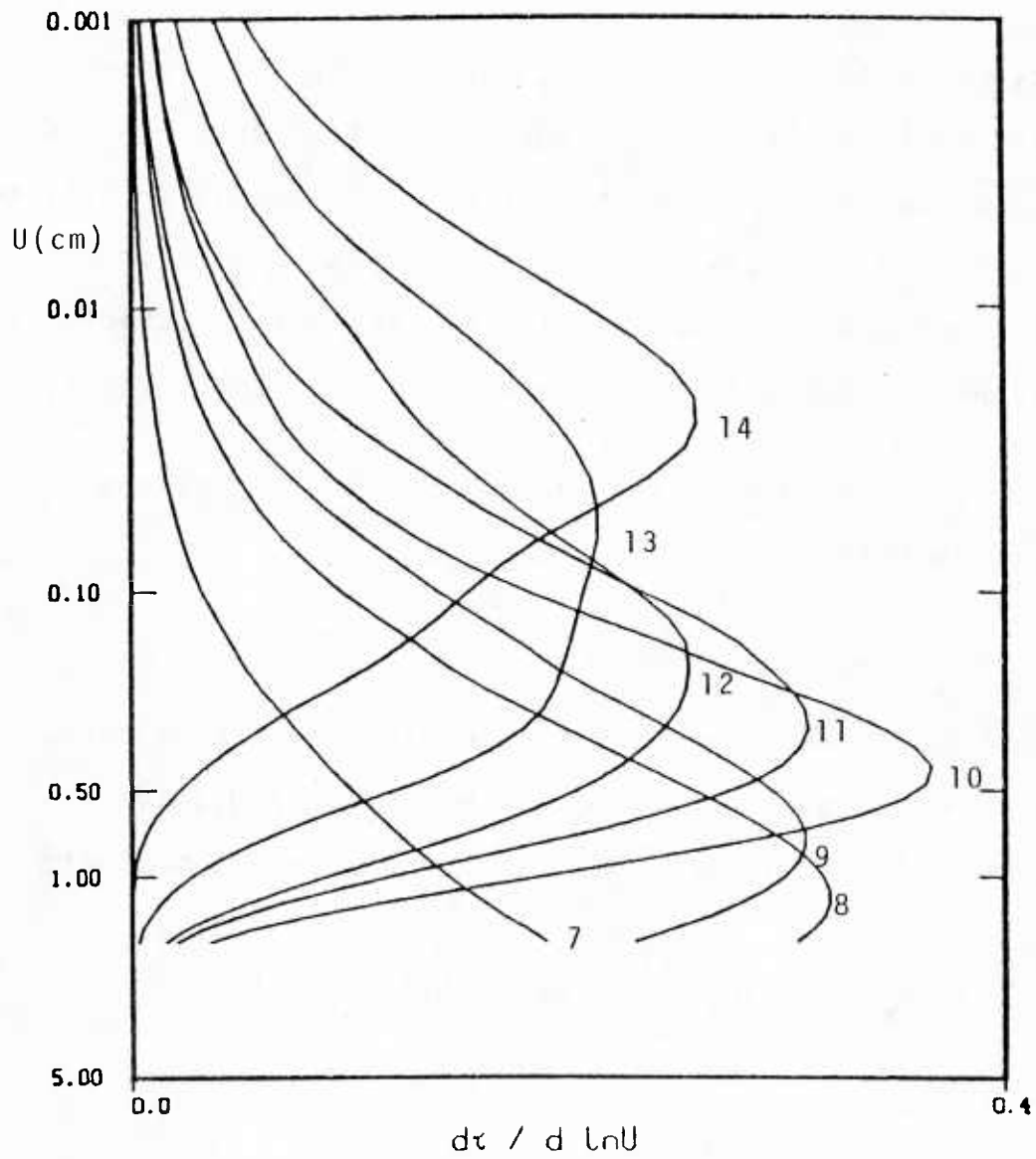

Figure 3.6. U-Space Weighting Functions, $\partial\tau_i/\partial \ln U$ -- Mid-Latitude Summer Profile

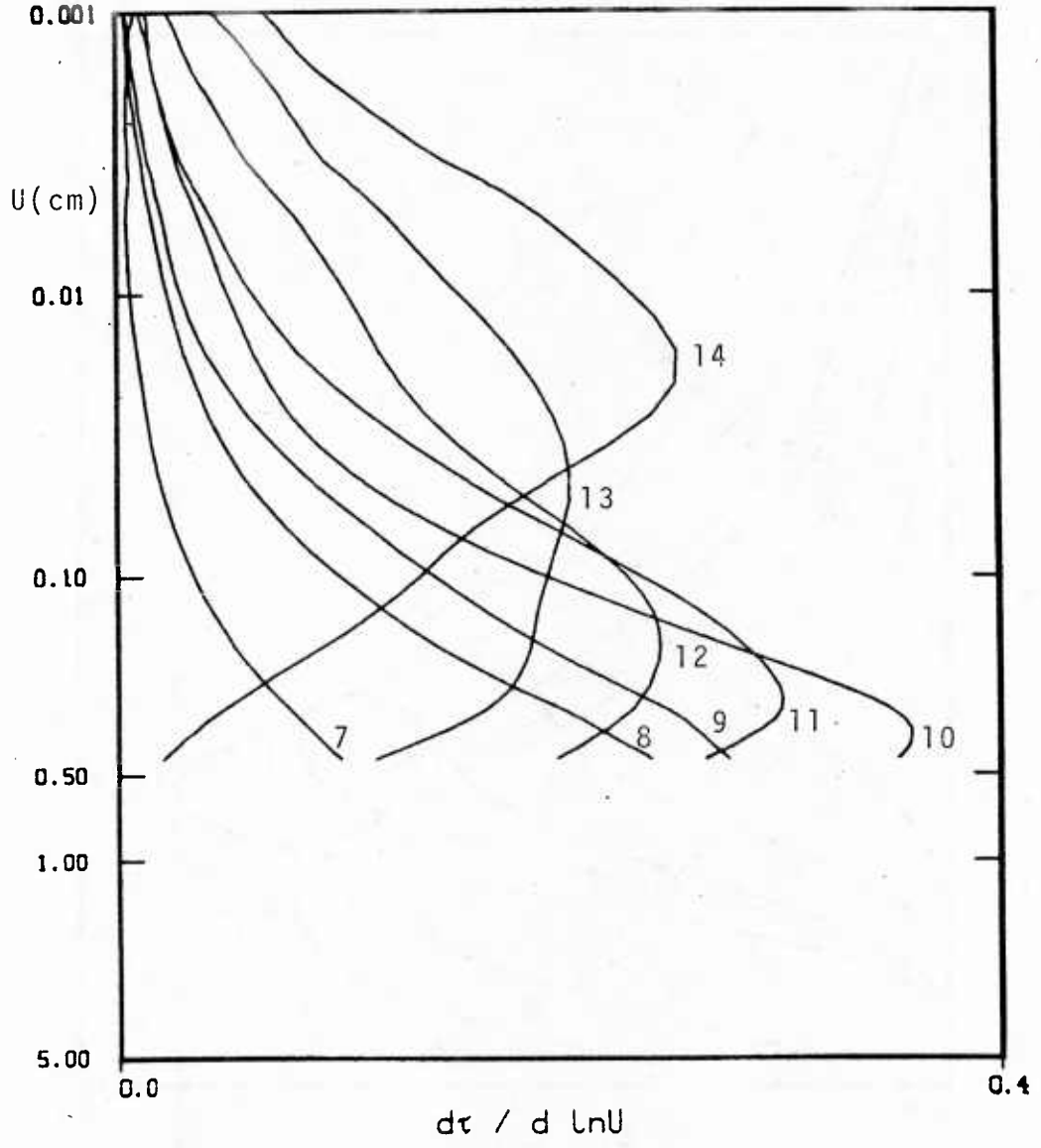

Figure 3.7. U-Space Weighting Functions, $\partial\tau_i/\partial\ln U$ -- Subarctic Winter Profile

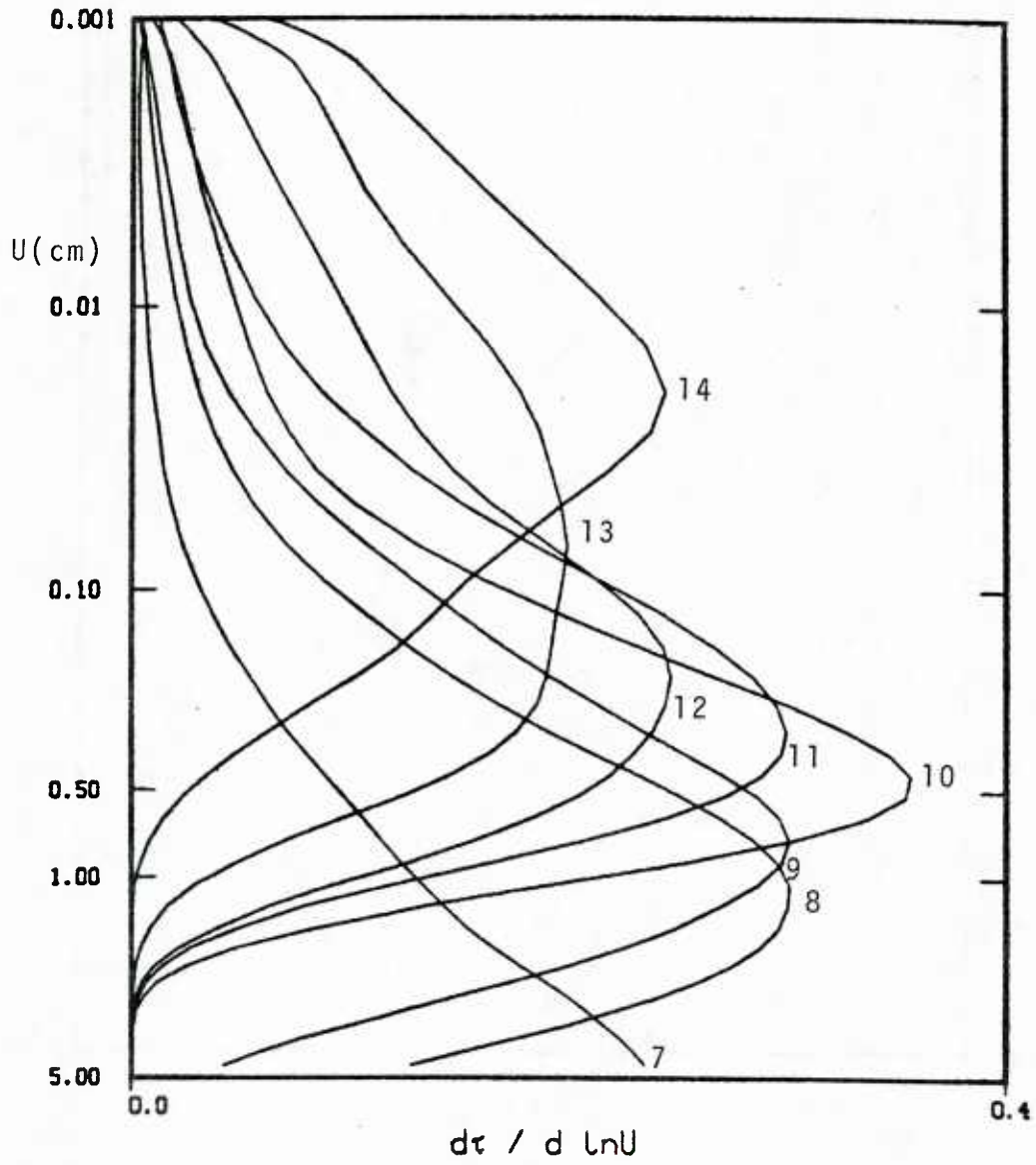

Figure 3.8. U-Space Weighting Functions, $\partial\tau_i/\partial\ln U$ -- Tropical Profile

level of the weighting function changes by an order of magnitude, from .5 cm H_2O for the arctic model to 5 cm for the tropical model.

This sensitivity is an indication that the temperature, pressure, and so-called memory effects on absorption for these bands are secondary to the total H_2O amount in the path. For channels in regions with absorption dominated by constant (or nearly constant) mixing ratio gases the functions plotted in pressure space and integrated absorber space are identical.

3.2 SENSITIVITY CALCULATIONS

Weighting functions indicate which levels of the atmosphere contribute most to the measured radiance. However, for remote sensing problems one is interested in the sensitivity of the measurement to changes in the desired parameter. A sensitivity that exceeds the noise level, as well as the effects of other undesirable and uncorrectable factors, is a necessary, but not sufficient condition for ultimately retrieving the desired quantity from the measurements.

The sensitivity of the SSH/2 water vapor channels was studied by dividing the atmosphere into layers and perturbing separately the values of temperature and water vapor amount in each layer. Radiances were computed for each channel for perturbation at all levels, and these were subtracted from the radiances of the unperturbed profile. By plotting these differences as a function of the level at which the perturbation was applied, one can see the

relative sensitivity of the channels throughout the atmosphere. Because all layers of our model atmosphere are not of a uniform thickness, the radiance differences were normalized by dividing by the thickness of the layer in kilometers. Because the amount of water vapor varies by many orders of magnitude from the bottom of the atmosphere to the tropopause, the water vapor was perturbed by an amount equal to 80% of the standard value at each layer. This 80% increase may result in unphysical profiles in the sense that relative humidities greater than 100% can occur, but since the physics of absorption is not affected by relative humidity, this procedure gives a reasonable indication of the sensitivity.

The sensitivity to water vapor amount was compared with the changes in observed brightness temperature due to decreasing the temperatue in each layer by 2°K. The 80% perturbation is a large change relative to the desired accuracy of 10%, but was selected due to the narrow 1 km layers to which these changes were made.

The sensitivity calculations were performed using a rapid algorithm for transmittances developed in an internally funded research program. The details of the algorithm are given in Appendix A.

Because of the non-linear nature of the problem the sensitivity is dependent on the base or unperturbed profile chosen. Figure 3.9 shows the response to an 80% increase in layer H_2O amount for a mid-latitude summer atmospheric profile. Increasing the

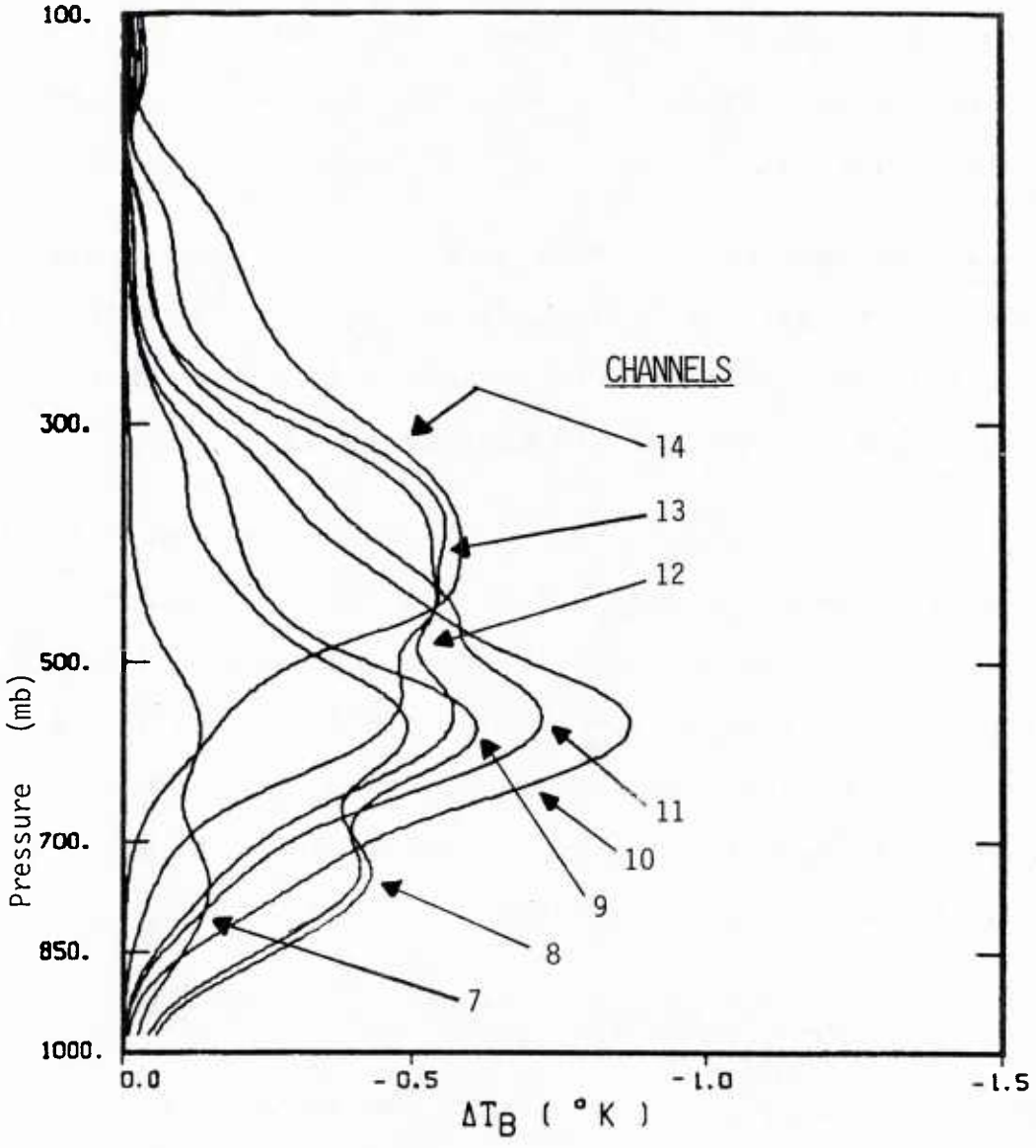

Figure 3.9. Sensitivity to an 80% Increase in Atmospheric Layer Water Vapor

amount of water vapor increases the absorption, causing the emission to come from higher and colder (in the troposphere) levels. Thus an increase in water vapor causes a decrease in observed brightness temperature. The peak of sensitivity occurs for all channels between 700 and 300 mb and the curves are much less spread out than the weighting function curves.

It is important to note that none of the channels have significant sensitivity near the surface; this occurs despite the large surface contribution to radiance for channels 7 and 8. This effect will be explained further in the next section.

Uncertainties in cloud cover and temperature also contribute noise that tends to mask changes due to water vapor effects. Figure 3.10 shows the sensitivity to perturbation by 2°K of the temperature for each layer. Although the peaks of these sensitivity curves are less than those for the water vapor sensitivity they are spread over a larger range of the atmosphere and some channels peak near the surface.

3.3 LACK OF UPPER AND LOWER ATMOSPHERIC SENSITIVITY

Figures 3.11, 3.12, and 3.13 show the temperature and H_2O sensitivity superposed for channels 8, 10 and 13 respectively. Channel 8 has the best H_2O sensitivity at the lowest levels, but even for this channel, below 850 mb, the H_2O sensitivity is less than the temperature sensitivity. The other channels show a greater H_2O sensitivity compared with temperature, but this advantage is confined to levels 400-600 mb.

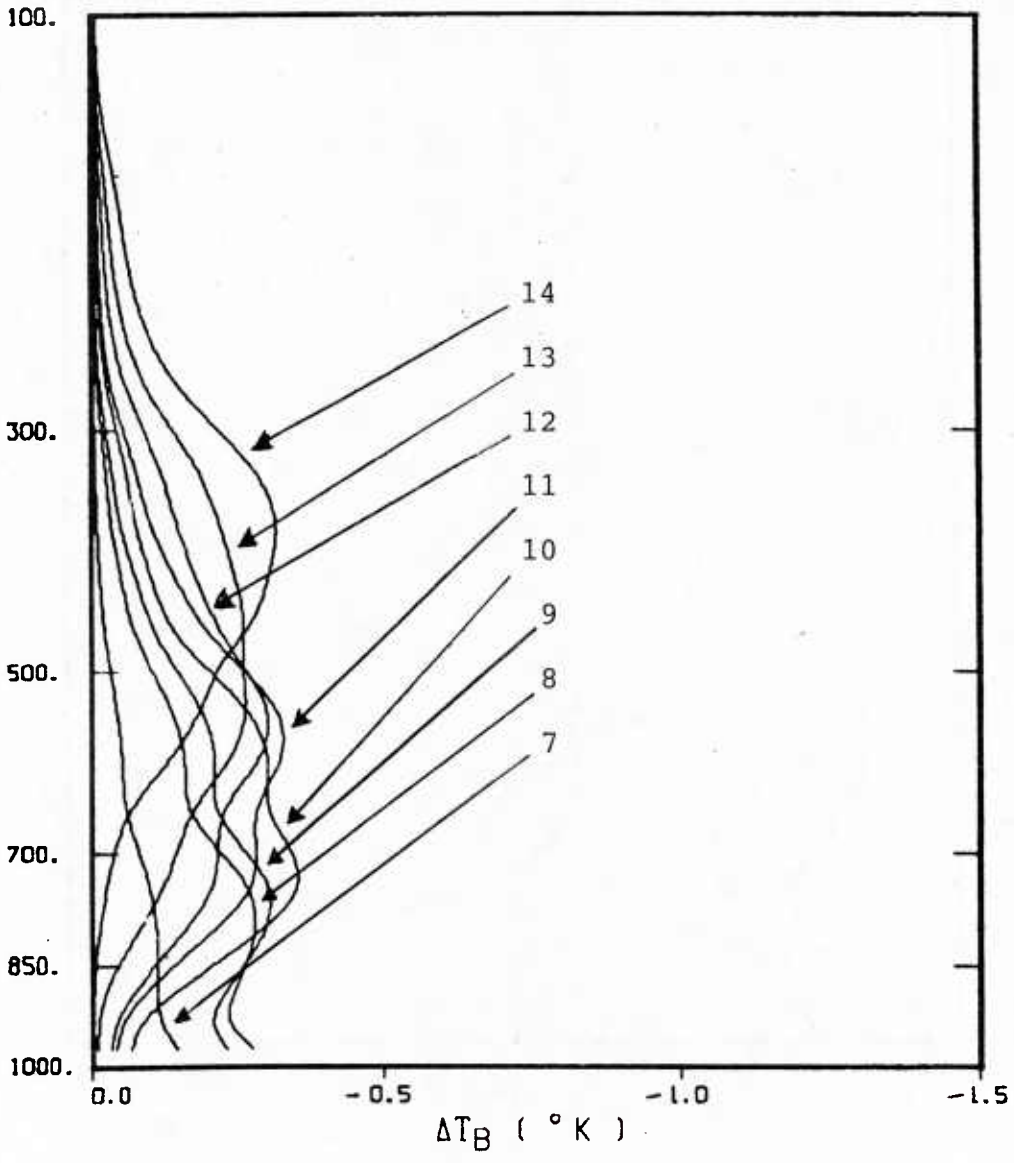

Figure 3.10. Sensitivity to a 2°K Decrease in Atmospheric Layer Temperature

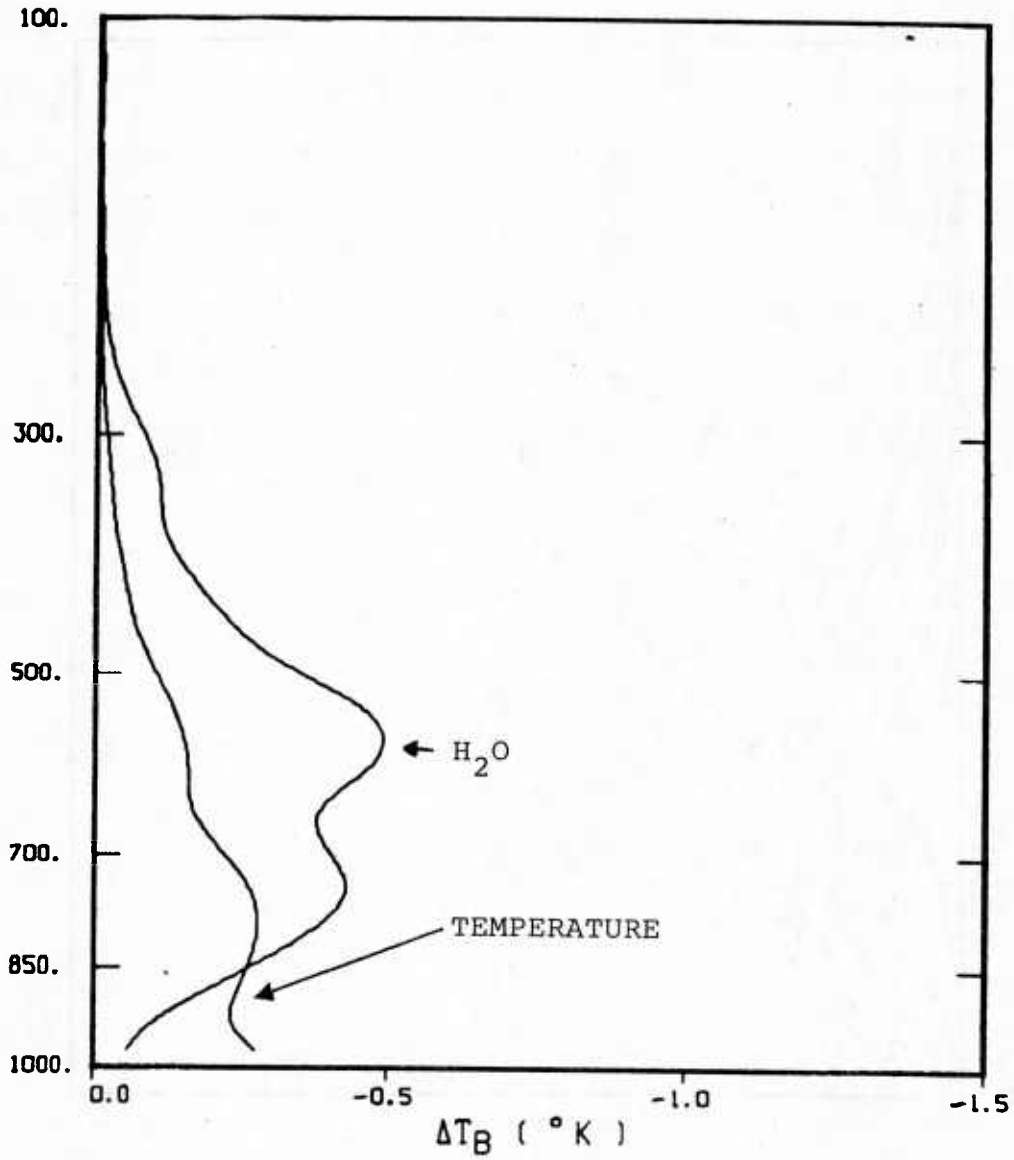

Figure 3.11. Temperature and H_2O Sensitivity of Channel 8

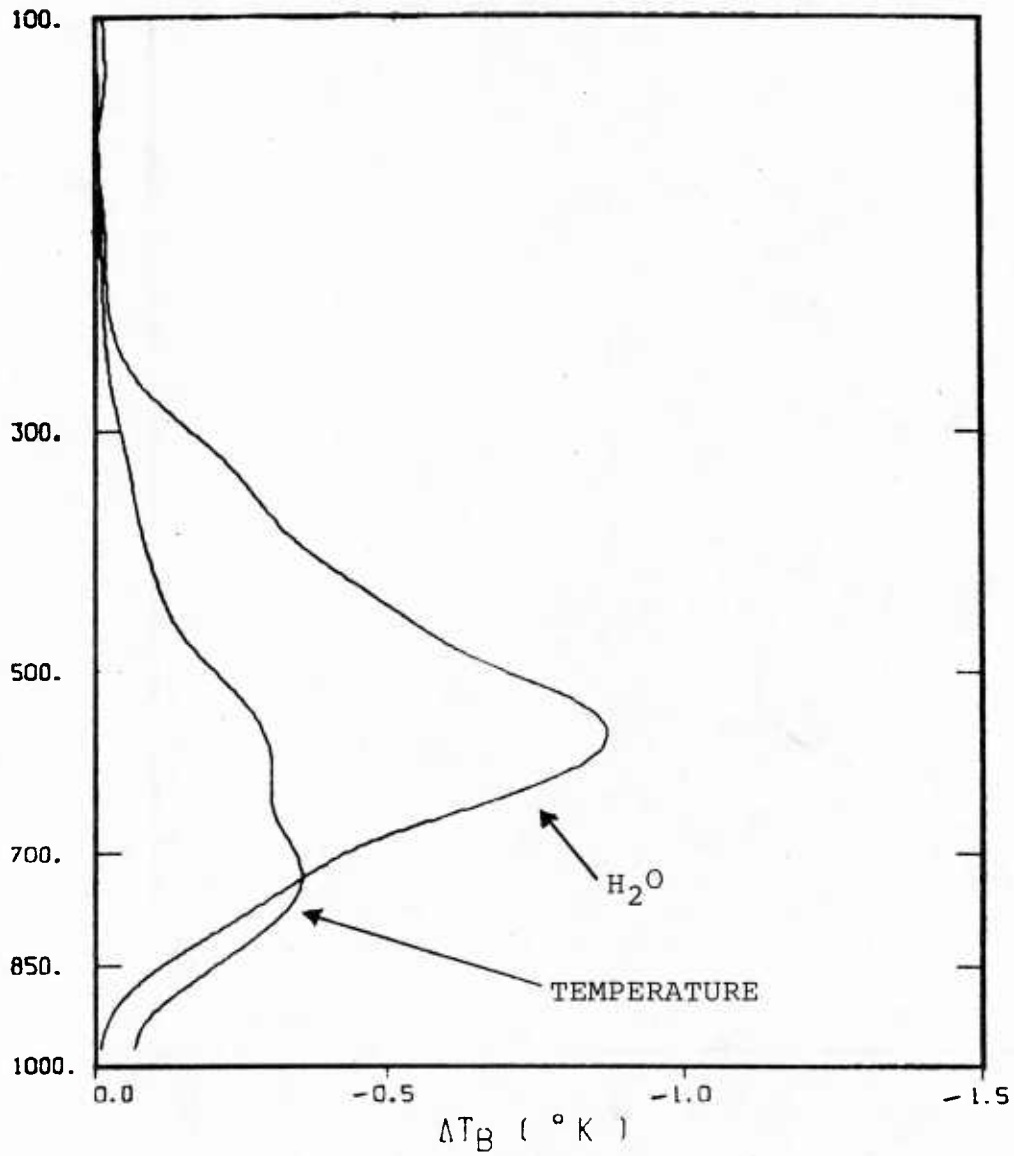

Figure 3.12. Temperature and H_2O Sensitivity of Channel 10

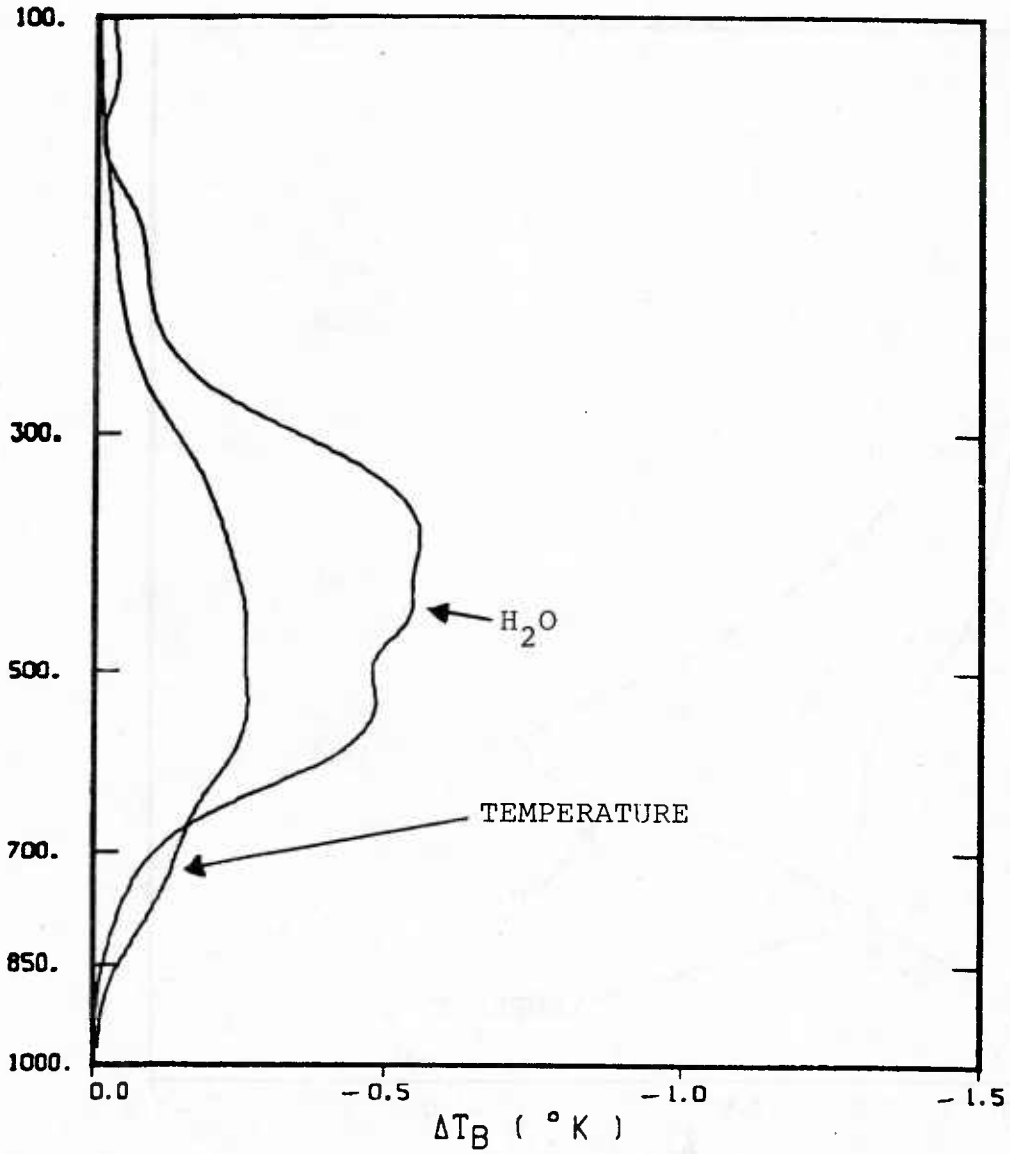

Figure 3.13. Temperature and H_2O Sensitivity of Channel 13

Figures 3.14 and 3.15 show the effect of a different atmospheric base profile on sensitivity. The temperature and water vapor sensitivity of channel 10 was plotted for both the mid-latitude summer profile used above, and a tropical profile. The temperature sensitivity is shifted to significantly higher levels in the tropical case but the effect on H_2O sensitivity is much less.

The lack of sensitivity near the surface to water vapor changes can be understood by rewriting the R.T.E. using integration by parts as,

$$r_i = \int_{B_{\bar{\nu}i}(P_{top})}^{B_{\bar{\nu}i}(Ps)} \tau_i(P)\, dB_{\bar{\nu}i}(p) + B_{\bar{\nu}i}[T(P_{top})] \qquad (4)$$

and discretizing it at J levels with level J the surface and level 1 at P_{top},

$$r_i = \sum_{j=2}^{J} \tau_i(P_j) \left.\frac{\partial B_{\bar{\nu}i}}{\partial T}\right|_{T(P_j)} (T(P_j)-T(P_{j-1}) + B_{\bar{\nu}i}[T(P_1)] \qquad (5)$$

Noting that the transmittance, $\tau_i(p_j)$, may be written,

$$\tau_i(P_J) = \prod_{k=1}^{J} \delta\tau_i(P_k) \qquad (6)$$

where $\delta\tau_i(p_k)$ is the effective transmittance from p_k to p_{k-1}, and if it is assumed that changes in water vapor amount at a given layer affect only the transmittance for that layer. This

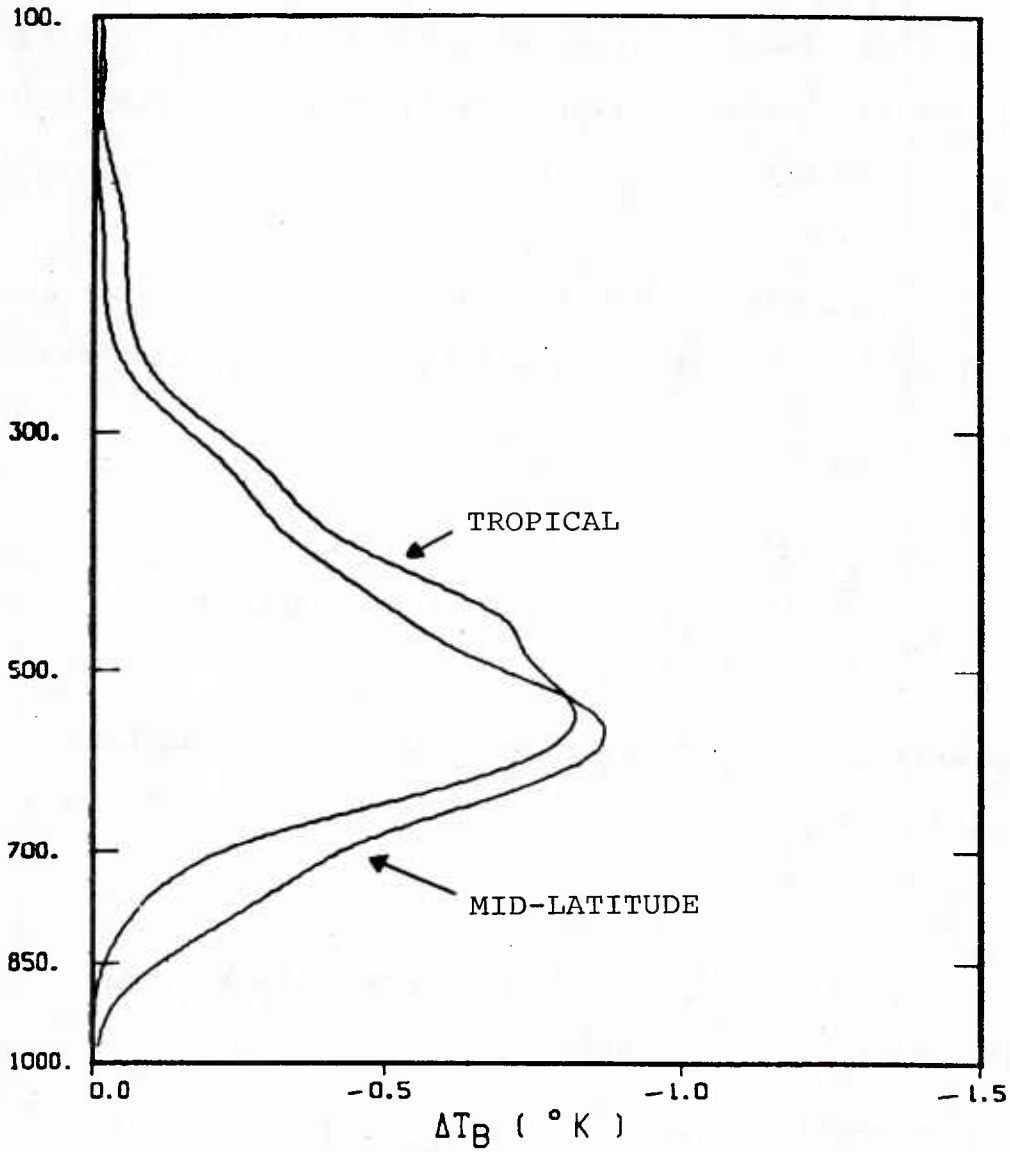

Figure 3.14. H_2O Sensitivity of Channel 10 to Mid-Latitude Summer and Tropical Profiles

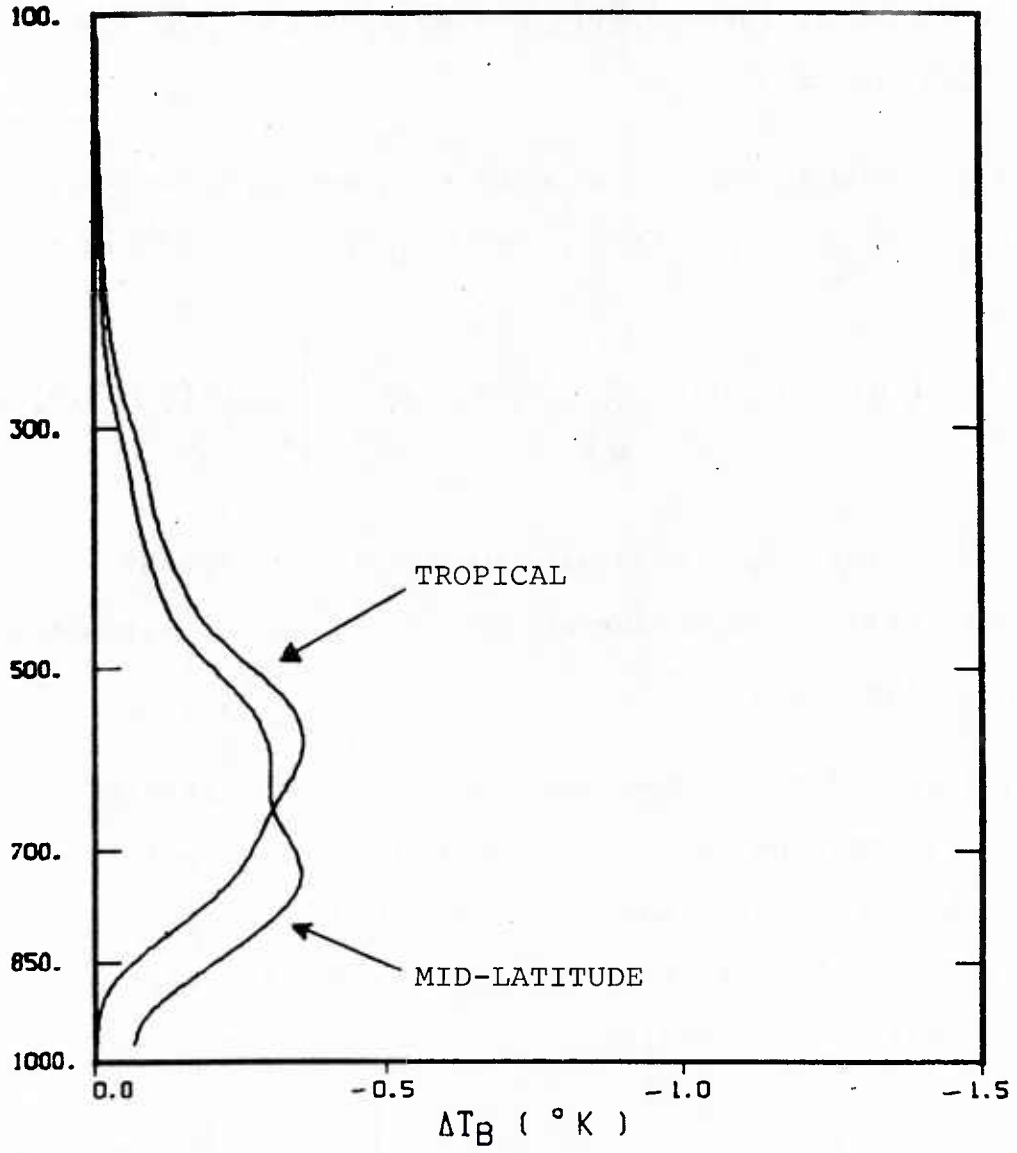

Figure 3.15. Temperature Sensitivity of Channel 10 to Mid-Latitude Summer and Tropical Profiles

approximation is a good one if the layers are narrow and the perturbations are small. Even for thick layers, effects in the layer transmittance at lower layers are smaller than the change at the layer perturbed.

The sensitivity in observed radiance to a change in water vapor mixing ratio q_k in the layer from p_k to p_{k-1} may be written,

$$\frac{\partial r_i}{\partial q_k} = \frac{\partial}{\partial q_k} [\ln(\delta\tau_i(P_k))] \cdot \sum_{j=k}^{J} \tau_i(P_j) \left.\frac{\partial B_{\nu i}}{\partial T}\right|_{T_j} \left[T(P_j) - T(P_{j-1})\right] \quad (7)$$

The first term on the right hand side of (7) is the change in effective layer optical depth for channel i and can be estimated from the rapid algorithm.

As expected, there is no response to a change at any levels where $\tau_i(p) = 0$. Changes near the surface are made up of few terms in the summation. Each term is weighted by the temperature lapse in that layer. For the case of the term nearest to the surface one writes,

$$\frac{\partial r_i}{\partial q_J} = \frac{\partial}{\partial q_J} [\ln(\delta\tau_i(P_J))] \cdot \tau_i(P_J) \left.\frac{\partial B_{\nu i}}{\partial T}\right|_{T_J} (T_J - T_{J-1}) \quad (8)$$

If the lowest layer is isothermal the response is again zero. Even if the lapse rate is not zero the single term in the summation results in less sensitivity than at higher layers which contain several terms. Thus, it can be seen that for infrared sounders sensitivity to water vapor will, in general,

be small at layers near the ground. The behavior exhibited by the SSH/2 is a property of all passive sounders used for constituent retrievals when the surface emissivity, ε, is near 1.

Such is the case for the entire infrared region and for microwave observations over land. In microwave observations over water, where ε is significantly smaller than unity, the sensitivity is greater, but other problems arise; the emissivity and skin temperature must be determined to a high accuracy.

SECTION 4.0

OUTLINE OF STUDY PLAN

4.1 IMPLICATIONS OF SENSITIVITY STUDY

The lack of sensitivity of any of the SSH/2 channels to water vapor in the lowest layers demonstrates that one cannot obtain direct information on H_2O at these levels from the SSH/2 radiances alone. However, other information is available. Physically we know that the relative humidity must be between 0-100%. (Actually it may exceed 100% slightly, but only in regions of high cloudiness that probably preclude retrievals anyway.) Thus if we can obtain the corresponding temperature profile from CO_2 channels or a microwave sounder we can place some limits on the allowable H_2O content. Statistical information obtained from in situ measurements (e.g., the radiosonde network) allows one to relate the water vapor in the middle troposphere, where direct information is available, to the amounts at lower layers. Statistical relationships can also be derived between the temperature, where again direct information is available even at lower layers, and the H_2O content. Thus this lack of lower atmospheric sensitivity does not preclude retrieval of water vapor there; it only makes it more difficult.

Such statistically derived profiles have the potential for improvement by a physically based solution of the R.T.E., but only in the region of high H_2O sensitivity (850-400 Mb). Our

approach thus consists of a statistical first guess improved by a non-linear relaxation technique.

4.2 STATISTICAL INVERSION

One of the most straightforward ways to use this additional information in obtaining a retrieval is to use a statistical inversion method. Several possible methods are:

(a) a multiple linear regression using only a subset of possible channels to insure invertability of the covariance matrix (screening regression)

(b) a multiple linear regression incorporating external constraints that add a regularization matrix for stability of the solution.

(c) a regression in an eigenspace

Before discussing the advantages and disadvantages of each of these methods, some features common to all will be described. These linear statistical techniques can all be written as,

$$q = Ct \tag{9}$$

where q is a vector of predictands, C is a matrix derived for each technique, t is a vector of predictors. The predictors may be any information that is related statistically to the quantity we desire. For example, the predictors may be observed radiances or brightness temperatures of water vapor

channels, radiances or brightness temperatures of CO_2 channels, water vapor or temperature information obtained from a numerical weather prediction model, or cloudiness information obtained from IR window and visible channels. Any combination of these or other parameters is possible. The stability of some methods limits the predictors that may be used, particularly when there is a high degree of interdependence between them.

For each method, the prediction matrix C is derived by using a set of SSH/2 observations that coincides with a set of radiosonde measurements. The radiosonde measurements are considered exact. Operationally, only infrequently do spacecraft passes exactly coincide with a radiosonde launch, so a criteria must be set that determines when these two observations are collocated closely enough in space and time to be included in the statistics. This set of dependent data is used to derive the linear prediction matrix, C.

To summarize, some of the common features of the three statistical techniques previously discussed are:

(1) all methods are linear

(2) a wide range of predictors and predictands is possible

(3) they require ground truth statistics to derive the solution matrix

A straightforward regression procedure, that predicts the water vapor at each level, q_i, as a function of the measured

brightness temperatures for each channel, suffers from several drawbacks. First, if all channels were used in the regression, the large degree of interdependence between them would result in an unstable solution. Elimination of several channels from the predictors in the regression would solve the instability problem -- at the expense of eliminating the small amount of independent information contained in the rejected channels. Second, the correlation between water vapor at various levels limits the number of independent pieces of information that may be obtained from the data. This number is certainly less than 24, the number of levels used in our calculations.

The eigenvalue-eigenvector method (EEM) developed by Smith and Woolf[1] solves both these problems. It enables one to include all channels in the regression procedure without instability and noise sensitivity problems. In addition, the correlation of water vapor amounts between layers is taken into account in such a way that variations not justified by the radiances measurements are not introduced.

The regression technique employing regularization can be shown to be equivalent to the EEM technique[10]. The Smith-Woolf technique was selected because with it the instability can be seen and eliminated more easily than with the regularization technique.

4.3 NON-LINEAR RELAXATION CORRECTION

The deviation of a level's mixing ratio, q_i, from its statistical mean, can be considered a function of the deviation of the eight channel brightness temperatures (T_B) from the value they would have for the statistical mean profile (ΔT_B). The matrix C expresses each q_i as a linear function of the eight T_B deviations, ΔT_B.

Higher order terms could, of course, be included. That is, each value of q_i could be expressed as the statistical q_i plus a power series in the eight ΔT_B's. The C matrix gives the coefficients in the linear terms; quadratic, cubic, and higher coefficients might also be generated.

Such a scheme would have the limitation of any power series expansion: it would be inaccurate for large arguments. Therefore it was decided to make the "non-linear" correction via a relaxation process . This involves computing a new set of brightness temperatures, a new set of ΔT_B's, with presumably smaller values, and from these, a correction to the first guess in q_i. One can then stop or make as many repetitions as necessary. The details of this correction method are in Section 6.

4.4 SIMULATION TECHNIQUES

As real observations are not yet available from the SSH/2, it is necessary to simulate a set of collocated observed brightness temperatures and atmospheric temperature profiles and moisture profiles.

A set of 1200 temperature and water vapor profiles obtained from NOAA/NESS[1] was used to derive and test both the statistical first guess profiles discussed in this section, and the relaxation algorithms. The profiles are divided into groups of 400, coming from arctic, tropical, and mid-latitude regions.

Radiances and brightness temperatures for channels 7-14 of the SSH/2 were simulated for these 1200 profiles using the rapid transmittance algorithm. The combined profiles and radiances were then available to derive the linear prediction matrices C. For this purpose the three climatological sets -- mid-latitude, arctic, and tropical -- were each divided into groups of 225 dependent profiles to derive the matrix C, and 75 independent profiles to test its accuracy. The remaining 100 profiles in each group were reserved for later unbiased tests that may be desired. The means and standard deviations for water vapor and temperature for the mid-latitude, arctic, and tropical 400 profile subsets are given in Tables 4.1 and 4.2. all radiative transfer calculations were made in a 24 level coordinate system, the twenty levels given in Tables 4.1 and 4.2, plus four at lower pressures (1 mb, 10 mb, 50 mb, and 100 mb). These four levels were included to accurately account for the small absorbtion due to constant mixing ratio gases.

Table 4.1 Water Vapor Statistics of the NOAA/NESS Data Set

Pressure (mb)	Water Vapor Mixing Ratio (g/kg)					
	Mid-latitude Profiles		Arctic Profiles		Tropical Profiles	
	Mean	Sigma	Mean	Sigma	Mean	Sigma
115	2.591E-03	3.243E-03	1.684E-03	2.675E-03	3.703E-03	2.528E-03
135	3.909E-03	4.671E-03	2.622E-03	4.001E-03	5.589E-03	3.797E-03
150	4.751E-03	5.554E-03	3.237E-03	4.874E-03	6.908E-03	4.807E-03
200	1.130E-02	1.347E-02	7.655E-03	1.158E-02	1.868E-02	1.556E-02
250	2.123E-02	2.721E-02	9.086E-03	1.090E-02	4.931E-02	3.347E-02
300	3.891E-02	5.194E-02	1.294E-02	1.596E-02	9.892E-02	6.422E-02
350	1.397E-01	1.722E-01	4.236E-02	4.824E-02	3.049E-01	2.016E-01
400	2.278E-01	2.889E-01	6.784E-02	8.162E-02	4.846E-01	3.431E-01
430	3.521E-01	3.889E-01	1.323E-01	1.498E-01	6.904E-01	4.715E-01
475	5.234E-01	5.501E-01	2.213E-01	2.672E-01	9.739E-01	6.925E-01
500	6.119E-01	6.379E-01	2.681E-01	3.339E-01	1.120E+00	8.144E-01
570	1.151E+00	9.540E-01	5.678E-01	5.318E-01	2.057E+00	1.197E+00
620	1.497E+00	1.210E+00	7.607E-01	6.901E-01	2.659E+00	1.532E+00
670	1.820E+00	1.460E+00	9.440E+01	8.451E-01	3.214E+00	1.865E+00
700	2.001E+00	1.605E+00	1.049E+00	9.359E-01	3.527E+00	2.060E+00
780	2.922E+00	2.056E+00	1.482E+00	1.218E+00	6.138E+00	2.265E+00
850	3.655E+00	2.594E+00	1.828E+00	1.519E+00	8.212E+00	2.735E+00
920	4.579E+00	3.185E+00	2.085E+00	1.835E+00	1.072E+01	2.896E+00
950	4.985E+00	3.540E+00	2.215E+00	2.010E+00	1.196E+01	3.062E+00
1000	5.635E+00	4.185E+00	2.424E+00	2.320E+00	1.393E+01	3.467E+00

Table 4.2 Temperature Statistics of the NOAA/NESS Data Set

Pressure (mb)	Temperature (°K)					
	Mid-latitude Profiles		Arctic Profiles		Tropical Profiles	
	Mean	Sigma	Mean	Sigma	Mean	Sigma
115	214.88	7.20	221.16	7.33	201.75	3.92
135	215.70	6.73	221.38	6.96	205.11	3.31
150	216.23	6.63	221.53	6.83	207.32	3.31
200	218.57	5.28	220.84	6.54	217.88	2.79
250	222.65	5.48	219.74	5.46	228.95	3.02
300	228.38	7.31	221.51	5.30	238.60	3.54
350	235.69	8.01	227.51	5.72	246.80	3.36
400	242.04	9.04	232.70	7.03	253.90	3.89
430	245.71	9.18	236.09	7.33	257.63	3.67
475	250.76	9.38	240.76	7.72	262.78	3.26
500	253.36	9.66	243.17	8.15	265.43	3.55
570	259.59	9.80	248.93	8.03	271.54	3.03
620	263.58	10.10	252.63	8.23	275.47	3.36
670	267.27	10.21	256.06	8.30	279.10	2.78
700	269.35	10.48	257.98	8.61	281.14	3.41
780	273.14	11.16	261.45	9.42	285.42	3.89
850	276.15	11.97	264.21	10.42	288.82	4.13
920	278.17	12.66	265.70	12.10	292.80	4.34
950	278.99	13.00	266.30	12.91	294.43	3.87
1000	280.29	13.94	267.26	14.55	297.00	5.01

In this study only H_2O channel brightness temperatures and tropospheric temperatures were used. Brightness temperatures are preferred in general to radiances because fewer scaling problems arise. Actual level temperatures, as opposed to CO_2 brightness temperatures, were used because they do not require a rapid algorithm to calculate transmittances and radiances.

SECTION 5.0

STATISTICAL FIRST GUESS

5.1 SMITH-WOOLF TECHNIQUE

The notation used for the first guess procedure is:

- n — number of predictors (# of channels plus # of temperatures)
- r — number of predictands (# of levels)
- s — number of dependent data samples
- m — number of eigenvectors selected for the predictands ($m \leq r$)
- q — number of eigenvectors selected for predictors ($q \leq n$)
- U — matrix of predictands, columns are H_2O profiles for s samples (r x s)
- T — matrix of predictors, columns are brightness temperatures and atmospheric temperatures (n x s)
- $\mathbf{U}^*$ — eigenvectors of UU^t (r x r)
- $\hat{U}^*$ — selected subset of first m eigenvectors of U^* (r x m)
- Λ — diagonal matrix whose elements are eigenvalues corresponding to columns of U^* arranged in decreasing magnitude (r x r)
- Λ^* — First m eigenvalues of Λ (m x m)
- $\mathbf{T}^*$ — eigenvectors of $\mathbf{T}\mathbf{T}^t$ (n x n)
- $\hat{T}^*$ — selected subset of first q eigenvectors of T (q x n)
- Λ_T — same as Λ corresponding to T^* (n x n)
- Λ_T^* — same as Λ^* corresponding to $\hat{T}^*$ (q x q)
- C — linear prediction matrix

The matrices $\mathbf{U}^*$, Λ, $\mathbf{T}^*$, Λ_T satisfy, $(UU^t) = U^*\Lambda U^{*t}$, $U^{*t}U = I$

and $(TT^t) = I$, where the superscript t denotes a transpose and I is the identity matrix.

By truncating U^*, Λ^* and T^*, Λ^*, to the largest m and q eigenvalues respectively, the matrix C may be written,

$$C = (1/s)(\hat{U}^* \hat{U}^{*t})(UT^t)(\hat{T}^* \Lambda_T^{*-1} \hat{T}^{*t}) \quad (10)$$

It can be shown that if we use all the eigenvectors (i.e. $m = T$, $q = n$) that (10) reduces to the ordinary least squares solution

$$C = U T^t (T T^t)^{-1} \quad (11)$$

Given a vector of observations, $\hat{t}$, a first guess profile, $\hat{q}$ is obtained from,

$$\hat{q} = C \hat{t} \quad (12)$$

The sensitivity of the ordinary least squares solution to errors is given by the condition number K. This is given by

$$K = \lambda_1/\lambda_n \qquad \text{where} \quad \lambda_i,\ i = 1...n$$

are the diagonal elements (eigenvalues) of Λ_T. Since the weighting functions of the SSH/2 are highly overlapping, the covariance matrix TT^t is usually singular or near singular.

This results in λ_i that rapidly approach zero as i increases and $\lambda_i >> \lambda_n$. Hence the condition number, K, is quite large. A large K means that small errors in the observed quantity **t** are mapped into large errors in the retrieved quantity **q**, resulting in solutions highly sensitive to noise[11]. It should be noted that due to round off effects in the computer, some degree of noise is always present, even for simulated radiances with no explicity added errors.

Now the advantage of the Smith-Woolf method can be seen: by truncating the sequence of eigenvalues, one reduces the condition number, and hence the sensitivity to noise.

5.2 FIRST GUESS PROGRAM IMPLEMENTATION

A program was written to implement the Smith-Woolf technique and test it using the set of profiles and corresponding brightness temperatures. The procedure is:

- Read parameters to control the run
- Compute covariance and cross covariance matrices for selected set of dependent profiles
- Compute eigenvectors and eigenvalues
- Select q and m (the number of eigenvectors of UU^t and TT^t respectively)
- Compute C matrix
- Loop for each profile in independent set
  - Calculate **q = Ct**
  - Correct so relative humidity is in range 0-100%
  - Calculate errors and update statistics on errors

- End Loop
- Print out summary of results and errors
- End Program

The first guess program has the following features:

- PREDICTORS — SSH/2 brightness temperatures and atmospheric level temperatures may be used in any combination
- PREDICTANDS — Water vapor was predicted in units of mixing ratios, integrated layer amount, and total amount from the top of the atmosphere to a given level.
- NOISE — Gaussian noise may be added to observed brightness temperatures and or level temperature estimates.
- DESATURATION — Retrieved profiles may be adjusted so relative humidity is within a given range for any level.
- NUMBER OF EIGENVALUES — One or several combination of U and T eigenvalues may be tested.

The choice of predictors is given in Table 5.1. Any combination of these quantities can be tested. In addition a test was made by averaging the tropospheric temperatures.

Table 5.2 is a list of the fractional variance explained by the first eight eigenvectors of mixing ratio and brightness temperature, given for the dependent subsets of mid-latitude, artic, and tropical profiles.

TABLE 5.1 Available Predictors for the Smith-Woolf First Guess Procedure

PREDICTOR NUMBER (CHANNEL)	PREDICTOR	
1	TEMPERATURE AT	300 mb
2		500 mb
3		620 mb
4		700 mb
5		920 mb
6		1000 mb
7	SSH/2 CHANNEL	7
8		8
9		9
10		10
11		11
12		12
13		13
14		14

TABLE 5.2 PERCENTAGE VARIANCE EXPLAINED FOR THE FIRST EIGHT EIGENVECTORS OF WATER VAPOR AND BRIGHTNESS TEMPERATURES

Eigenvectors of 24 Predictands (H_2O Levels)

Eigenvector Number	Mid-Latitude % of Variance Explained		Arctic % of Variance Explained		Tropical % of Variance Explained	
	(1)	(2)	(1)	(2)	(1)	(2)
1	87.83	87.83	93.35	93.35	83.66	83.66
2	9.42	97.25	5.30	98.65	11.42	95.08
3	1.92	99.17	0.93	99.58	3.39	98.47
4	0.71	99.88	0.37	99.95	1.40	99.87
5	0.07	99.99	0.02	99.98	0.11	99.98
6	0.04	100.00	0.02	100.00	0.01	99.99
7	0.00	100.00	0.00	100.00	0.01	100.00
8	0.00	100.00	0.00	100.00	0.00	100.00

Eigenvectors of 14 Predictors

Eigenvector Number	Mid-Latitude % of Variance Explained		Arctic % of Variance Explained		Tropical % of Variance Explained	
	(1)	(2)	(1)	(2)	(1)	(2)
1	88.31	88.31	88.11	88.11	59.04	59.04
2	5.44	93.75	5.49	93.60	25.95	84.99
3	3.81	97.56	3.34	96.94	5.54	90.53
4	1.19	98.75	1.70	98.65	3.74	94.27
5	0.44	99.19	0.69	99.34	2.29	96.55
6	0.41	99.59	0.32	99.65	1.49	98.04
7	0.22	99.81	0.19	99.85	1.05	99.09
8	0.09	99.91	0.09	99.94	0.70	99.76

(1) is the variance explained for each eigenvector

(2) is the cumulative variance explained for eigenvector up to current one

5.3 EVALUATION OF FIRST GUESS RESULTS

The accuracy of the first guess algorithm was judged by considering several factors:

(1) the root mean square error of water vapor at each level as a fraction of the mean of the dependent profiles (RMS) at that level.

(2) the mean square error at each level as a fraction of the variance at that level of the dependent profiles (fractional unexplained variance, FUV).

(3) the RMS error of the total integrated water vapor from the surface to the top of the atmosphere derived from the predicted profile.

(4) the FUV of the total integrated water vapor derived from the predicted profile.

The RMS error is mathematically defined as:

$$\mathrm{RMS}(q) = \left[\frac{1}{N}\sum_{i=1}^{N}(\hat{q}_i - q_i)^2\right]^{\frac{1}{2}} / \bar{q} \qquad (13)$$

where the sum is over the N independent profiles, $\hat{q}_i$ is the predicted quantity for observation i, q_i is the exact quantity, and $\bar{q}$ is the mean of q over the dependent set of profiles. The FUV is defined as:

$$\mathrm{FUV}(q) = \left[\frac{1}{N}\sum_{i=1}^{N}(\hat{q}_i - q_i)^2\right] / \mathrm{var}(q) \qquad (14)$$

where var(q) is the variance of the dependent profiles.

Statistically FUV is a more meaningful measure of the performance of the first guess procedure because it tells us how much we were able to reduce the natural variations of the atmosphere. For FUV = 0 one has a perfect set of retrievals. A FUV = 1 means a worthless set of retrievals in the sense that one would do just as well by using the climatological mean.

5.4 FIRST GUESS PROGRAM RESULTS

The statistical first guess procedure was evaluated by running controlled tests to determine optimal settings for the various options of the program. These tests selected a basic control run from which one factor was changed and the effects on the resultant errors were then compared.

The following factors were investigated:

(1) optimal units for predictands
(2) the optimal predictors
(3) the effects of random noise added to the predictors
(4) the behavior for the three climatological subsets: mid-latitude, arctic, and tropical.

The control run that was held fixed for all four tests, was selected with the following parameters:

- water vapor was predicted in units of mixing ratio
- temperatures at all six levels in Table 5.1 and the 8 SSH/2 water vapor channels were used as predictors

- gaussian noise of 1°C was added to the temperature predictors and the brightness temperature noise level was set by the SSH/2 noise specifications in Table 3.1 (this is referred to as the low noise case)
- mid latitude profiles were selected

Tables 5.3-5.6 give the results for four tests.

Table 5.3 shows the effects of varying the units of the predictand. The integrated water vapor amount to a given pressure, U(p), gives significantly better results at most levels. This is due to the cancellation of errors of different signs, an effect that is not present when only level (q) or layer (ΔU) water vapor is predicted. A better indication of the overall accuracy is given by U_S, the total precipitable water vapor to the surface. This is the same as U(1000 mb). Mixing ratio, q, did somewhat better than integrated water vapor, U, and layer water vapor, ΔU. However, these differences are probably not significant. Tests run with several sequences of random noise generated from different seeds, but with the same statistical properties (standard deviation and bias), indicate that variations in FUV of 0.02 to 0.04 can be due to random fluxuations.

Table 5.4 shows the effects of using various predictors to predict mixing ratio. The use of temperature values alone does significantly worse than using temperature information and the H_2O brightness temperatures. Using the H_2O channels alone gives poor results, particularly at upper levels. This result is

Table 5.3 Effects of Various Predictands on First Guess Procedure Accuracy

Units of Predictand	Fractional Unexplained Variance pressure (mb)						Normalized RMS Error pressure (mb)					
	1000	850	700	500	300	U_s	1000	850	700	500	300	U_s
q	.231	.335	.176	.308	.693	.115	.336	.392	.338	.596	1.05	.227
U (p)	.137	.125	.155	.238	.538	.137	.244	.258	.332	.539	.856	.244
ΔU (p)	.261	.314	.184	.289	.609	.153	.348	.378	.345	.579	.965	.261

q is mixing ratio (g/kg), U (p) is integrated water vapor from top of atmosphere to pressure p, ΔU (p) is layer H_2O from P_i to P_{i-1}, U_s is the derived total precipitable water vapor to 1000 mb (same as U (1000) for U (p) case).

Table 5.4 Effects of Various Predictors on the First Guess Procedure Accuracy

Channels Used		Fractional Unexplained Variance pressure (mb)						Normalized RMS Error pressure (mb)					
Temp.	H_2O	1000	850	700	500	300	U_S	1000	850	700	500	300	U_S
1-6	7-14	.231	.335	.176	.308	.693	.115	.336	.392	.338	.596	1.05	.227
1-6	NONE	0.296	0.551	0.588	0.610	1.116	0.388	0.380	0.503	0.617	0.839	1.329	0.391
NONE	7-14	0.237	0.418	0.438	0.438	0.925	0.274	0.340	0.438	0.533	0.712	1.210	0.305
(1 5)	7-14	0.196	0.326	0.226	0.265	0.735	0.128	0.309	0.387	0.382	0.553	1.078	0.212
1-6	7	0.301	0.528	0.479	0.504	1.030	0.335	0.384	0.492	0.557	0.763	1.277	0.369

Temperature and Humidity channels are same as in Table 5.1.

(1-5) designates the mean of temperature channels 1-5 was used as a predictor.

Other parameters are same as for control run.

Table 5.5 Effects of Various Noise Levels on First Guess Procedure Accuracies

Noise Levels	Fractional Unexplained Variance pressure (mb)						Normalized RMS Error pressure (mb)					
	1000	850	700	500	300	U_s	1000	850	700	500	300	U_s
None	.246	.351	.172	.297	.696	.125	.346	.401	.334	.586	1.05	.240
NO T, H_2O INST	.246	.349	.161	.297	.704	.121	.347	.400	.323	.586	1.06	.238
1.5°T, 1.0° H_2O	.268	.376	.291	.316	.743	.184	.362	.415	.434	.605	1.08	.277
1°T, H_2O INST	.231	.335	.176	.308	.693	.115	.336	.392	.338	.596	1.05	.227

H_2O INST refers to instrument specified noise levels given in Table 1.1

Other parameters are same as in control run.

Table 5.6 Effects of Various Climatological Profile Subsets of First Guess Procedure Accuracies

Climatological Subset	Fractional Unexplained Variance pressure (mb)						Normalized RMS Error pressure (mb)					
	1000	850	700	500	300	U_s	1000	850	700	500	300	U_s
Arctic	.151	.187	.398	1.39	.907	.179	.351	.345	.530	1.25	1.10	.192
Mid-latitude	.231	.335	.176	.308	.693	.115	.336	.392	.338	.596	1.05	.227
Tropical	.452	.399	.166	.234	.994	.191	.151	.207	.236	.345	.605	.334

Other parameters are same as in control run.

somewhat surprising as we expect that the lack of temperature information would show up most notably near the surface where the H_2O channels lack sensitivity. The reason may be that channels 7 and 8 give a good indication of the temperature at the lowest atmospheric levels, whereas the lack of temperature information in the upper and middle troposphere is more sigificant.

The effect of different noise levels is given in Table 5.5. Remembering that differences of about .02 in FUV are not significant we can see that noise becomes a significant effect only at the highest levels of 1.5°K temperature and 1°K in H_2O channel brightness temperatures. This is not surprising since the EOF regression technique is relatively insensitive to noisy measurements, as long as the dependent data used to generate the matrix C also contains the same noise levels as the independent set used to verify the accuracy.

In Table 5.6 the three climatological subsets, mid-latitude arctic, and tropical were investigated. Because of differing means and variances it is difficult to compare the accuracy of the three sets. The best overall behavior in terms of FUV was obtained by the midlatitude profiles which had FUV $\approx$ .3 or better up to 400 mb. Arctic profiles gave good accuracies below 700 mb but had an anamolously bad region around 500 mb. This may be due to the rapid decrease of H_2O with altitude around threse levels. Tropical profiles had moderately poor results near the surface with very good results (FUV $\approx$ .2) from about 500-850 mb.

SECTION 6.0

PHYSICALLY BASED RETRIEVALS

6.1 INTRODUCTION

One characteristic of statistical techniques, such as the Smith-Woolf method, is that there is no constraint that the predicted profile corresponds with the observed radiances, even within the noise limits of the system. The possibility arises that statistically derived retrievals of water vapor may be improved by correcting them to reduce the differences between observed radiances and those predicted from the profiles using the R.T.E. Such a task is likely to be a delicate one because of the limited sensitivity of the H_2O channels of the SSH/2. One must be sure that the corrections do not increase the error, particularly in regions of low sensitivity where noise is likely to have a large effect.

Such a physically based approach, involving solving the radiative transfer equation, has been investigated by Chahine[2], and Smith and Howell[12] among others. Unlike statistical procedures, physical retrievals require that the transmissive and radiative properties of the atmosphere be known for the instrument channels. Operationally, this requires careful calibration utilizing ground truth data. Computational requirements are generally greater than for linear statistical procedures.

Two such physically based retrievals using a non-linear relaxation technique were investigated. The basic procedure for both techniques consists of the following steps:

(1) Given a set of observed brightness temperatures T_{B_i}

(2) Set n = o and obtain a first guess profile $q^n(p)$ from the statistical technique.

(3) Compute the brightness temperatures $\hat{T}_{B_i}$, corresponding to the profile, $q^n(p)$.

(4) If $|| \hat{T}_{B_i} - T_{B_i} || < \varepsilon$, where the norm is taken over all channels, then exit (solution is $q^n(p)$). (Have our residuals converged to within the preselected tolerance, ε?)

(5) Compute $q^{n+1}(p) = f(q^n(p), \Delta T_{B_i})$.

n = n + 1 (Updated the profile based upon the previous iteration and the computed residuals)

(6) Go to Step 3

In addition, one must add checks to insure that the results in terms of residuals of T_B do not diverge, and that one does not continue to iterate indefinitely when neither converging nor diverging.

The basis of each technique lies in the way that the correction (Step 5.) is applied.

The first method that we tested uses the approach of Chahine, by correcting the water vapor amount at selected pressure levels and then interpolating and extrapolating to the remaining levels.

The second approach applies the corrections directly to the coefficients multiplying the eigenvectors obtained from the first guess procedure. These techniques and the results are discussed in the following sections.

6.2 THE FIXED LEVEL CORRECTION METHOD

In this technique, we followed the approach of Chahine for temperatures and constituent retrievals. Seven tropospheric pressure levels were selected at which to apply corrections. These levels are listed in Table 6.1. In order to reduce the effects of noise, the corrections at each of these levels was based on the weighted sum of the residuals for three channels. Layer water vapor amount q_i was updated as follows:

$$q_j^n = q_j^{n-1} + \gamma_j \sum_{k=7}^{14} W_{jk} F_{jk} \Delta T_{B_k} \qquad (15)$$

where,

$$F_{jk} = \frac{\partial T_{B_k} / \partial q_j}{\sum_{j=1}^{24} \left[\frac{\partial T_{B_k}}{\partial q_j} \right]^2}$$

TABLE 6.1 FIXED LEVEL RELAXATION WEIGHTS

LEVEL (j)	P_j (MB)	CHANNEL NUMBER							
		7	8	9	10	11	12	13	14
8	200	0	0	0	0	0	1/3	1/3	1/3
10	300	0	0	0	0	0	1/3	1/3	1/3
12	400	0	0	0	0	1/3	1/3	1/3	0
14	475	0	0	0	1/3	1/3	1/3	0	0
16	570	0	0	1/3	1/3	1/3	0	0	0
18	670	0	1/3	1/3	1/3	0	0	0	0
20	780	1/3	1/3	1/3	0	0	0	0	0
22	920	1/3	1/3	1/3	0	0	0	0	0

Because of the non-linear nature of the problem, if one makes too large a correction, the updated value of q may be so far from the true value that subsequent iterations might not approach the true solution. In general, one wishes to damp the correction. However, if one chooses γ too small, the solution may converge but very slowly. Tests indicated that $\gamma = 1/3$ provided a good balance between stable behavior and rapid convergence, for most cases.

The W_{jk} were chosen by giving a weight of 1/3 to the three channels with weighting functions peaking nearest the level p_j. Table 6.1 gives the weights W_{jk} for each level.

The term F_{jk} gives the sensitivity of changes in brightness temperature at that level relative to the total sensitivity at all levels. The derivatives were estimated from the rapid algorithm (see Appendix A) and recomputed for each step.

Once the water vapor amounts at these seven layers were updated, it was necessary to construct an entire profile from them. The final procedure adopted was:

1. Leave 1000mb unchanged from the first guess.
2. Linearly interpolate between 200mb and 1000 mb
3. Preserve the shape of the first guess profile for levels above 200mb by making adjustments to these levels proportional to the adjustment made at 200mb.

Accuracy was seldom improved by iterating after the residuals decreased to or below the noise level. Therefore, the trial value of the profile becomes the final answer, and the relaxation stops, when:

1. The residuals in six of the eight sounding channels are below 1 1/2 times the standard deviations of the noise in those channels;

or when:

2. The median (fourth highest) residual is 3/4 the standard deviation of the noise in that channel.

The exact form of this test follows from trial and error rather than any philosphical considerations. A random noise generator that outputs noise for eight channels will likely compute one or two very noisy radiances. So the routine stops when most residuals are below tolerance, assuming that those remaining out of tolerance are the very noisy ones and should therefore be ignored.

On any iteration the algorithm tests to see whether the residuals have increased or decreased. As with the tolerance test, some provision must be made for one or two noisy channels. Specifically, the trial solution is assumed to be converging if:

1. the residuals have decreased for six of the eight channels; and

2. the sum of all the residual's absolute values has decreased.

If neither of the above tests is met, the next iteration is rejected and the last trial solution is output as the final answer.

Another feature incorporated into the relaxation algorithms is a relative humidity correction. After each iteration, the water vapor at each level was adjusted to keep the relative humidity between 0-100%.

6.3 RELAXATION IN THE SPACE OF EOF's

Any profile in the 1200 profile set (and, presumably, nearly any observed profile) can be represented to a high accuracy as a linear combination of a seasonal average plus a few EOF's. This suggests that a good way to improve on the First Guess Algorithm, which calculates the expansion coefficients of the EOF's by expressing them as a linear combination of the observed brightness temperatures, would be to relax in the space of these expansion coefficients. This procedure removes the need for the interpolation and extrapolation of the fixed level method.

The basic approach in this technique is to relax in the space of expansion coefficients used in expressing the trial solution. Let a first guess profile be expressed as the sum of N EOF's,

$$q^{\circ}(P_j) = \sum_{\ell=1}^{N} a_{\ell}^{\circ} q_{\ell}^{*}(P_j) \tag{16}$$

where

$q^*_{\ell}(p_j)$ is the ℓ'th eigenfunction at p_j.

The coefficients a_{ℓ}^{n} are then generated from the previous iteration for channel k as follows

$$a_{\ell}^{n} = a_{\ell}^{n-1} + \gamma_{\ell}(\partial T_B / \partial a_{\ell}) \Big/ \sum_{i=1}^{N} (\partial T_{B_k} / \partial a_i)^2 \tag{17}$$

The derivatives $\partial T_{Bk}/\partial a_{\ell}$ are estimated from the rapid algorithm.

The weights γ_{ℓ} are selected for each EOF to insure stability. We know from our sample profiles that the first EOF explains most of the variance, with rapidly diminishing amounts explained

by succeeding EOF's. This means, on average, that the expansion coefficients decrease in magnitude as ℓ increases. To prevent the higher order coefficients from growing too rapidly one chooses successively smaller γ_ℓ's as ℓ increases. This behavior was obtained by choosing $\gamma_\ell = (1/\beta)^\ell$. $\beta = 3.5$ was selected after running several tests.

The small number of parameters adjusted suggests an alternative use of the divergence test. We compute a provisional correction in the three expansion coefficients based on only one channel's residual. Call this residual $(\hat{T}_B^n - T_B^n)$. Then the divergence test will tell us whether this provisional correction should be adopted. If so, we make the correction and apply the tolerance test; if not, we leave the profile unchanged. In either case (if the tolerance test is not met) we go on to another channel and compute another correction. This scheme is incorporated into the final form of the program shown schematically in Figure 6.1.

The convergence test and the relative humidity correction remain the same as for the fixed level correction scheme.

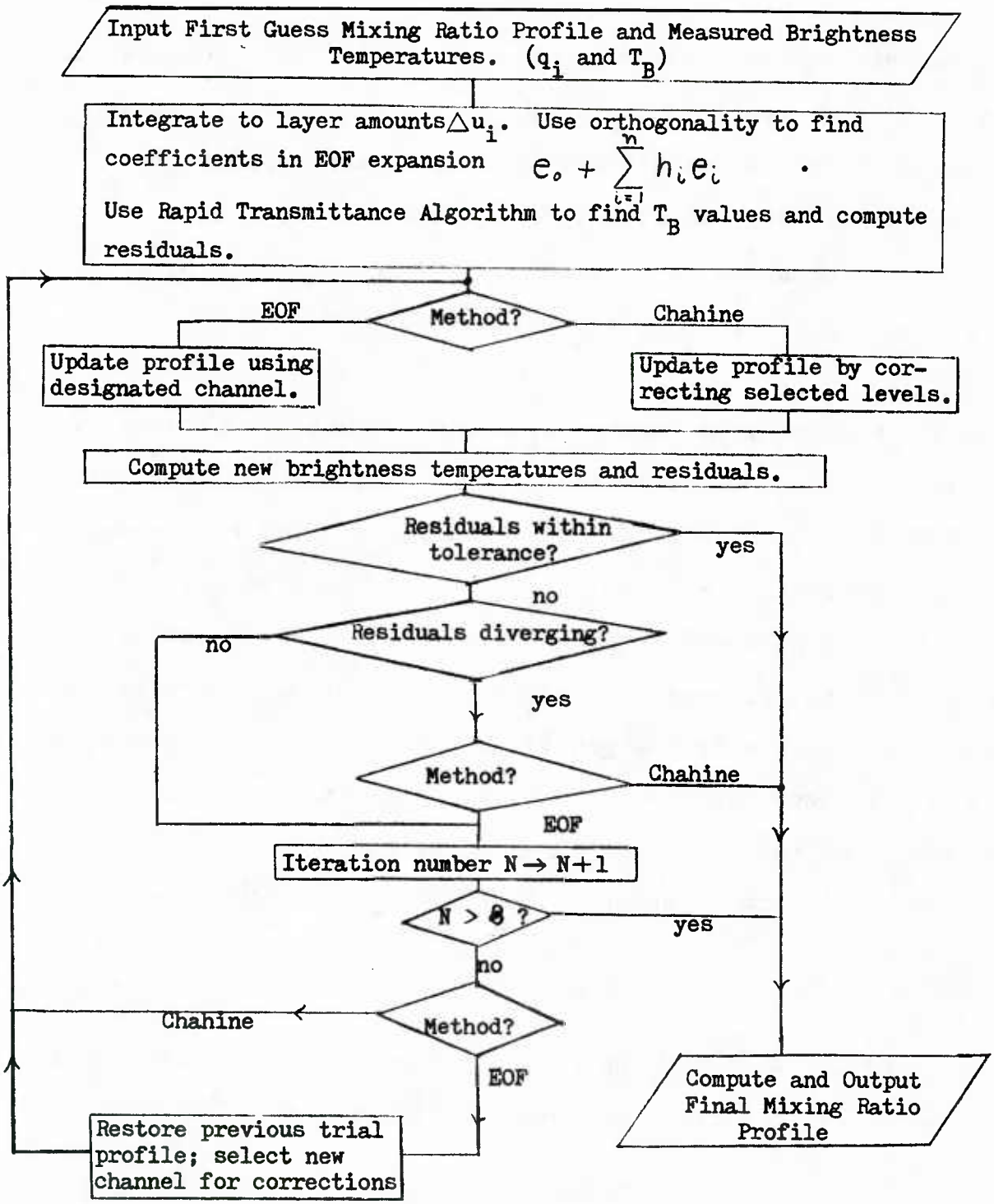

Figure 6.1 Flow Chart of the Non-linear Relaxation Algorithm

6.4 RELAXATION ALGORITHM RESULTS

The three climatological sets of mid-latitude, arctic, and tropical profiles were then tested with the two relaxation algorithms described above. The noised corrupted radiances were obtained, and the statistical first guess profile was passed to one of the two relaxation procedures. The relaxation algorithms then corrected the first guess moisture profiles, and the accuracies were computed. These were compared with the accuracy of the first guess itself. Figures 6.2 to 6.5 shows the results of the relaxation procedures.

Figure 6.2 gives the improvement for the mid-latitude set of profiles for the case of 1°K temperature noise and the SSH/2 instrument noise given in Table 3.1 (the instrument noise case). The Figures 6.3, 6.4 and 6.5 give results for the higher noise levels of 1.5°K temperature, and 1°K H_2O channel noise (the atmospheric noise case). The plots are of fractional unexplained variance as a function of altitude. The solid line gives the first guess algorithm alone, the dashed line the EOF Relaxation scheme, and the unconnected circles the fixed level correction scheme.

When the EOF method was used, an expansion truncated at three EOF's gave the best results for mid-latitude and arctic profiles. The tropical profiles required four EOF's, however.

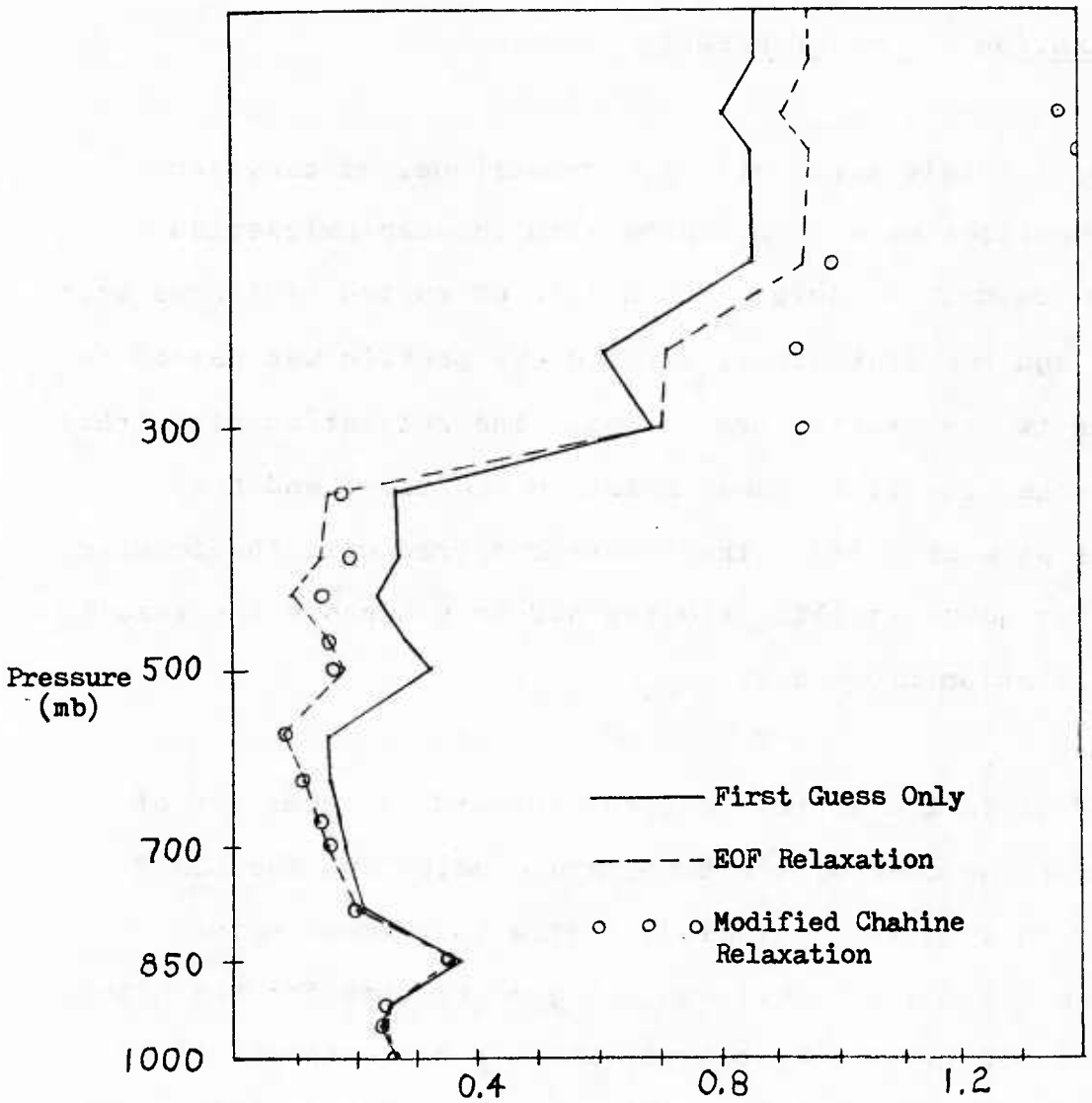

FIG. 6.2 COMBINED FIRST GUESS AND RELAXATION RESULTS FOR SIMULATED MIDLATITUDE PROFILES WITH ADDED INSTRUMENT NOISE

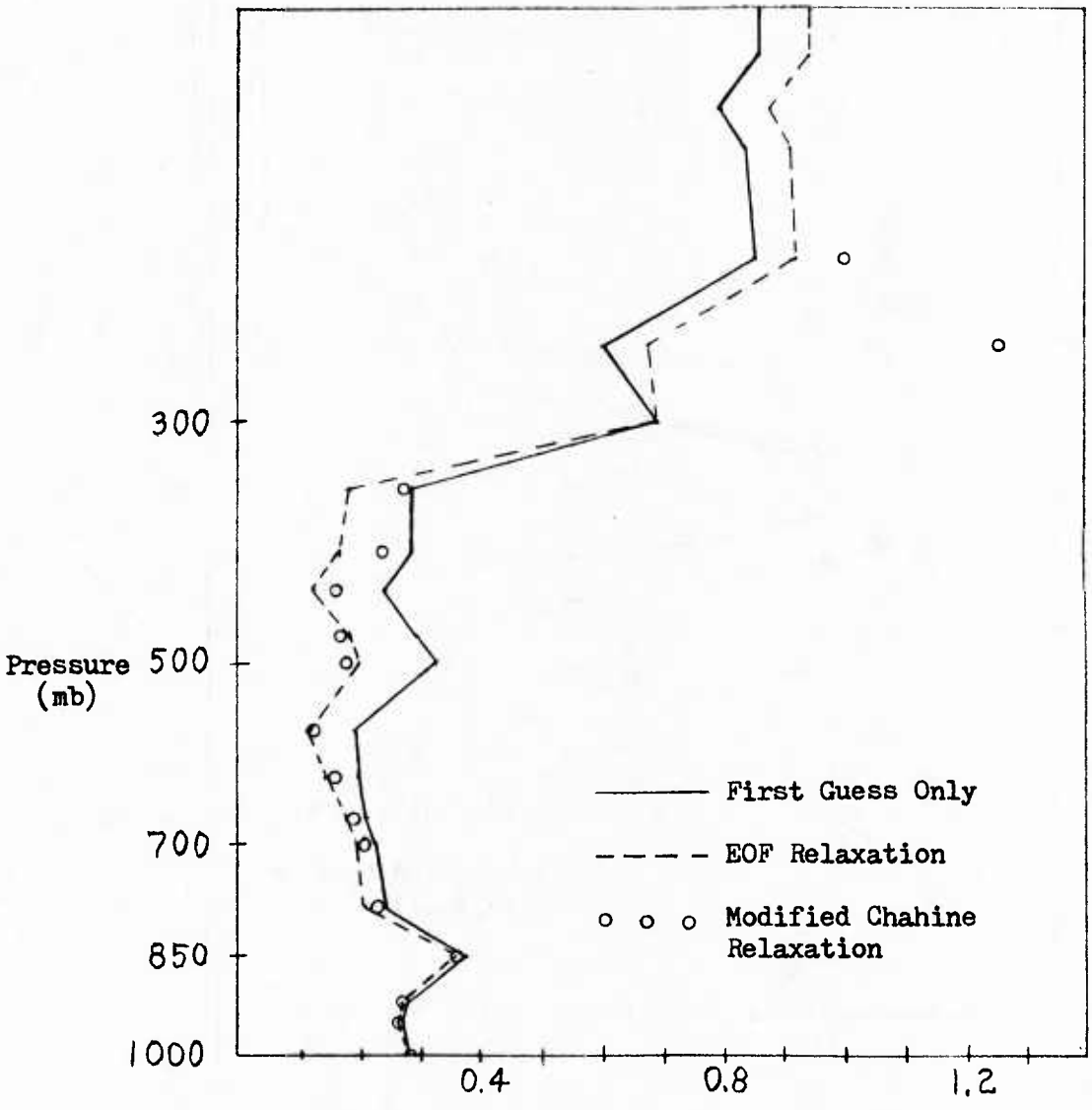

FIG. 6.3 COMBINED FIRST GUESS AND RELAXATION RESULTS FOR SIMULATED MIDLATITUDE PROFILES WITH ADDED ATMOSPHERIC NOISE

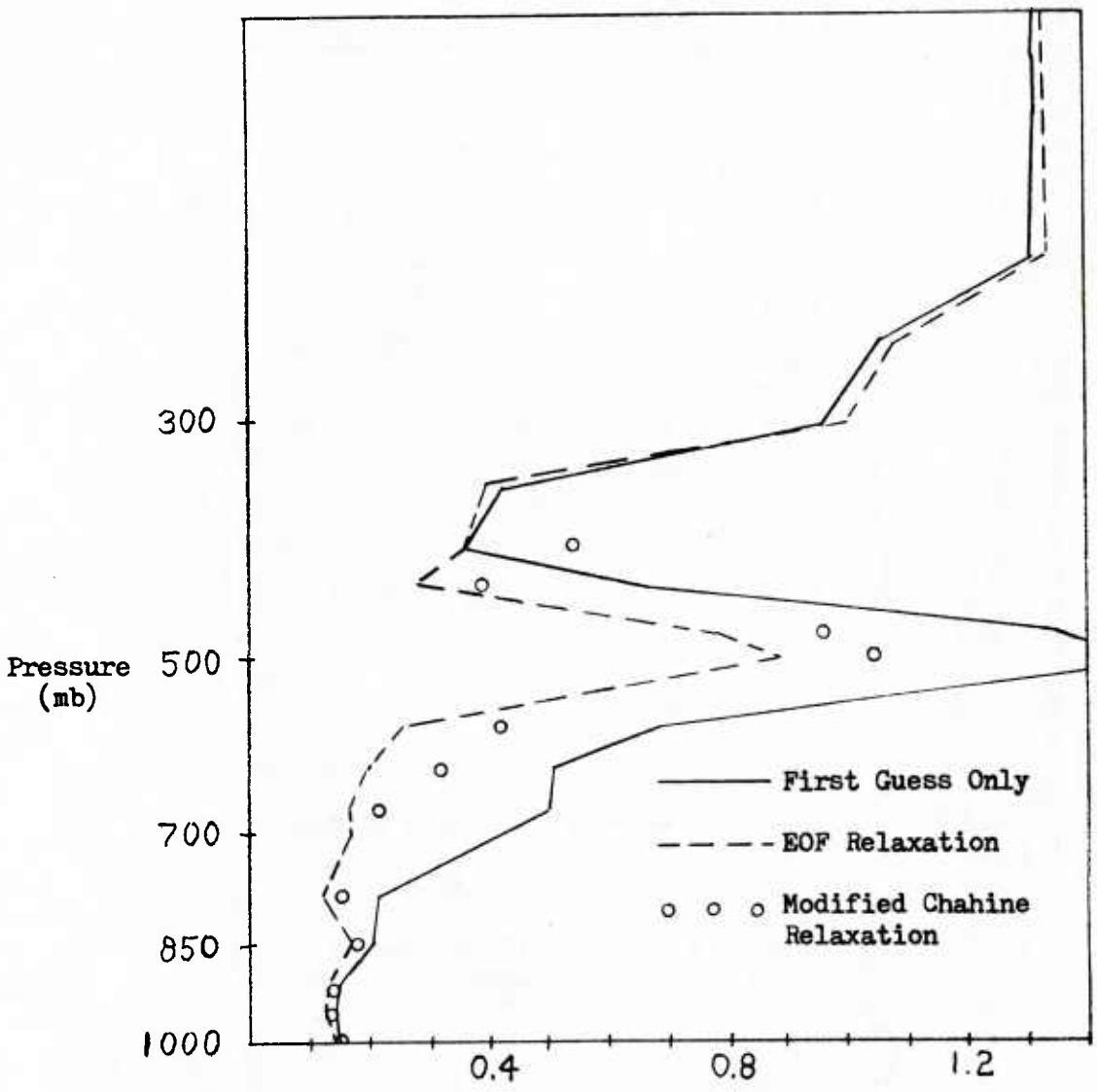

FIG. 6.4 COMBINED FIRST GUESS AND RELAXATION RESULTS FOR SIMULATED ARCTIC PROFILES WITH ADDED ATMOSPHERIC NOISE

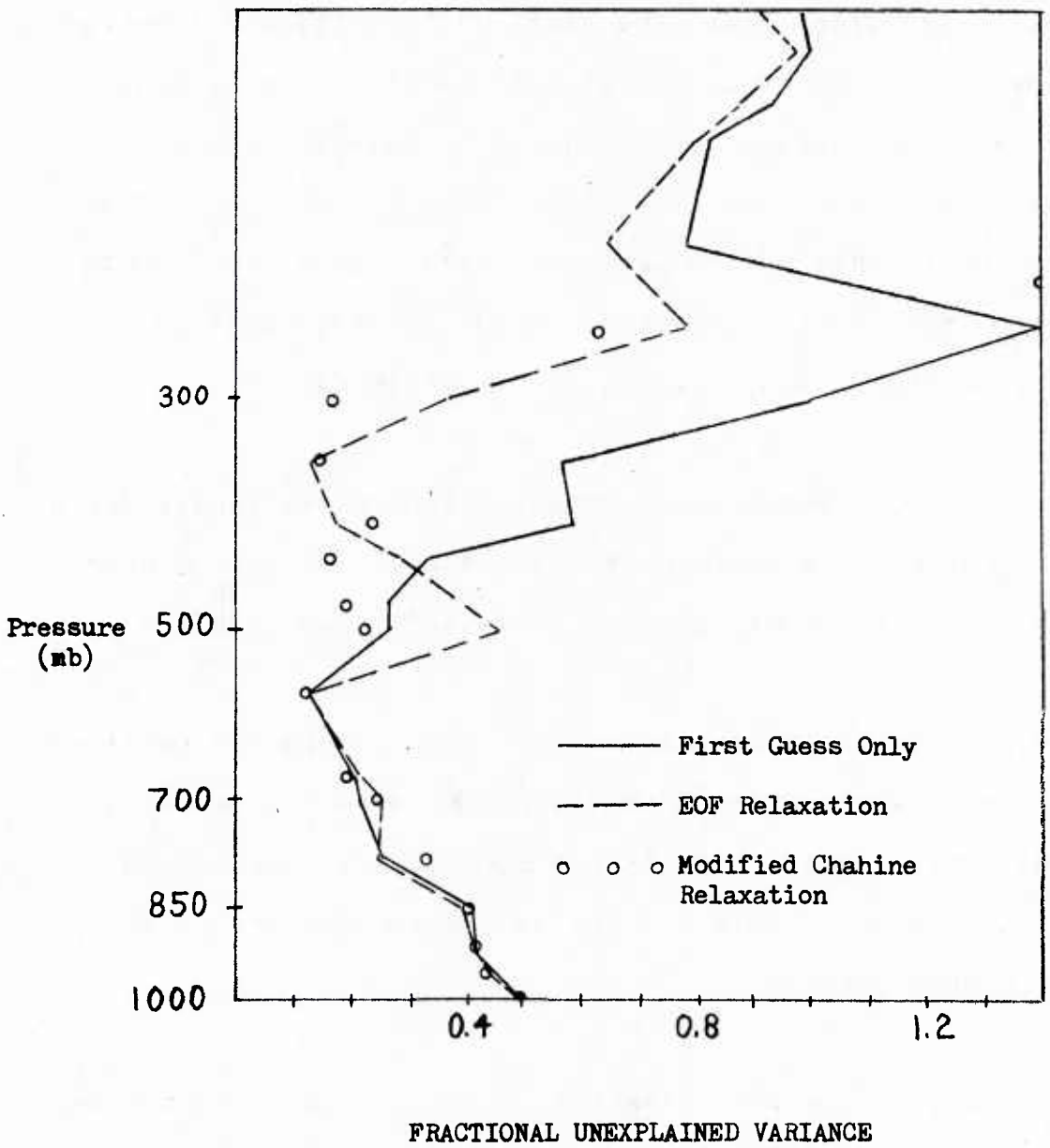

FIG. 6.5 COMBINED FIRST GUESS AND RELAXATION RESULTS FOR SIMULATED TROPICAL PROFILES WITH ADDED ATMOSPHERIC NOISE

Both relaxation algorithms give small but significant improvements for the mid-latitude set at both levels of noise from 400-700 mb. The surface levels showed no change. Levels above 300 mb indicated some decrease in accuracy but the first guess only results in this region were poor also. Such behavior is expected by the sensitivity study which indicated that only middle tropospheric improvements can be expected.

Figure 6.4 showed improvement at most tropospheric levels for an arctic atmosphere. Results were even improved at 500 mb where the first guess procedure yielded anomalously bad results.

Figure 6.5 gives tropical results. No improvement was obtained below 600 mb. The results from 300-600 mb were significantly improved. This upward shift is not unexpected, because the larger H_2O amounts in this set shifts the sensitivity of the SSH/2 to higher levels.

For the most part the two relaxation techniques yielded the same overall accuracy. The EOF scheme tended to be more stable particularly at higher levels, where it seldom degraded the results above 300 mb significantly, something the fixed level scheme often did. This is not surprising because the EOF scheme constrained the results to be in the space spanned by the first 3 or 4 eigenvectors. The magnitude of these vectors is, in general, quite small at the upper levels. Corrections, which

include ones that improve as well as degrade the results, were small at the higher levels. The EOF scheme also eliminates the need for the complicated interpolations used in the fixed level method. For these reasons the EOF technique is to be preferred.

SECTION 7.0

CONCLUSIONS

The water vapor channels of the DMSP SSH/2 sounder have been analyzed and their sensitivity to water vapor changes throughout the troposphere have been estimated. The eight H_2O channels measure radiation emitted throughout the troposphere from the surface to ~300 mb with a high degree of overlap. Their sensitivity to changes in water vapor content is concentrated over a much smaller region (for a mid-latitude profile the peaks in sensitivity range from 600-400 mb). The sensitivity approaches zero near the surface.

This lack of surface sensitivity was shown to be a property of all infrared passive thermal emission remote measurements of constituent content, not just of the SSH/2. From this analysis it is seen that the standard weighting functions $d\tau/d\ln p$ are not the appropriate means to evaluate water vapor sounding instruments, but rather sensitivity curves.

This lack of sensitivity by the SSH/2 water vapor channels, and indeed of all passive IR water vapor sounders, places severe limits on the direct information available on water vapor near the surface, as well as total precipitable water. This does not preclude indirectly obtaining water vapor profiles down to

the surface using statistical relationships. Such statistical relationships rely on the inherent correlations between temperature and water vapor amounts at a given level, and the correlation between water vapor at upper tropospheric levels (where direct information is available) and the near surface layers.

The regression technique developed by Smith and Woolf was selected to provide statistical retrievals. A simulation study was then performed using subsets of a group of 1200 atmospheric temperature and water vapor profiles. For realistic noise conditions total precipitable water amounts with an RMS error of .23 (root mean squared error/mean of dependent set) was found for a mid-latitude set of profiles. This corresponds to a fractional unexplained variance (FUV) of .12 (mean squared error/variance of the dependent set). The profiles obtained had RMS errors below .4 at most levels below 300 mb, corresponding to FUV's from .18 to .34.

Two non-linear relaxation improvement techniques, a fixed level correction scheme and an EOF relaxation scheme, were tested for their ability to improve the first guess results. Significant improvements in accuracy were obtained at most levels where the SSH/2 channels were sensitive. Measured in terms of FUV the improvements were generally .07 or greater. Of the two techniques that have been studied the EOF approach yielded more stable results, particularly at pressures below 300 mb.

APPENDIX A

RAPID ALGORITHM FOR SSH/2 TRANSMITTANCE

1. Introduction

The inversion of the radiative transfer equation to obtain temperature or absorber amount by a physical retrieval method requires that first one be able to solve the forward problem: given the vertical structure of temperature and absorber(s) determine the radiance that would be measured by each of the channels of the instrument in question. If the assumption of local thermodynamic equilibrium (L.T.E.) is valid, and scattering is unimportant, then the problem reduces to the accurate determination of transmittances for the instrument channels.

The calculation of transmittances can be obtained accurately by the computationally expensive line-by-line technique. With this method the primary source of error is uncertainties in the line parameters, and lack of knowledge of the continuum absorption.

If the accuracy of the line-by-line method is not adequate, empirical corrections can be made if adequate ground truth data are available. The lengthy computations in the line-by-line technique, however, preclude its use in obtaining the large number of transmittances required by a physical inversion method.

A computationally efficient method for determining atmospheric transmittances of the SSH/2 was thus developed. This rapid algorithm uses a line-by-line program to generate a set of dependdent transmittances for twenty five model atmospheres. The line-by-line program was provided by Goddard's Laboratory for Atmospheric Sciences[7] and modified and adapted for use on our system.

The twenty-five dependent profiles were used to generate a multivariate least squares model which is able to quickly calculate the SSH/2 transmittances (and thus the observed radiances) with sufficient accuracy for our purposes. The terms of the least squares model were chosen by a combination of physical intuition and trial and error. Once coefficients for the model were derived employing the dependent data test, a test was performed with twelve widely varying independent profiles. The details of the model and an evaluation of its accuracy are given in the following paragraphs.

2. Generation of Dependent and Independent Transmittance Data Sets

The modified line-by-line transmittance program was used to generate transmittances for a sample of 25 dependent and 12 independent profiles with which the rapid algorithm was generated and tested. The basis for this test was a set of 1200 profiles of temperature and water vapor obtained from the National Environmental Satellite Service.[1] This set contains a diverse set of profiles with 400 profile subsets each from mid-latitude, arctic, and tropical atmospheres. Means and standard deviations were computed for the entire set and for each 400 profile subset and are given in Table 4.1 and 4.2.

For the dependent data set of profiles it was desired to account for a wide range of possible variations in the atmosphere. This could be assured by taking a large number of realistic profiles from the 1200 profile tape, 100 or more for each channel. An "exact" transmittance calculation of 100 atmospheric profiles for

the eight channels, where the width of each channel is 30-40 cm^{-1}, requires a large amount of computational time. Instead we constructed 25 artificial profiles that contained a wide variation in both temperature and humidity.

The twenty five artificial profiles were constructed as follows:

First a set of 5 temperature profiles consisting of: (1) the mean of the 1200 profile set; (2) a profile reduced by one standard deviation (s.d.) at each level from the mean; (3) a profile varying from one s.d. above the mean at the top to one s.d. below the mean at the bottom; (4) a profile varying from one s.d. below the mean to one s.d. above the mean at the bottom; and (5) a profile everywhere increased by one s.d. from the mean.

Second, a set of 5 water vapor profiles were constructed as above, but a value 80% of the mean mixing ratio at each level was used instead of the standard deviation.

Finally, the twenty five artificial atmospheres were constructed by taking all possible combinations of the above five temperature and five moisture profiles.

It must be noted that not all profiles so constructed are realistic in the sense that relative humidities greater than 100% can and do occur. However, since the physics of absorption is dependent on absolute absorber amount, and not its relative saturation, and the purpose of the profiles is to generate a linear regression model, this should not be a problem.

The independent data set was chosen by selecting four profiles from each of the three groups on the tape. The transmittances for SSH/2 channels 7-14 were then calculated for the dependent and independent profiles and saved for later use.

3. Linear Regression Model

The effective layer optical depth was predicted with a regression model. For the layer p_i to p_{i-1} the effective layer optical depth is defined as follows:

$$K_i = -\ln \{\tau(P_i)/\tau(P_{i-1})\} \qquad (A1)$$

For a single frequency the effective layer optical depth is identical to the layer optical depth:

$$K_i = -\ln \{\tau(P_i \text{ to } P_{i-1})\} \qquad (A2)$$

but for the wide channels of the SSH/2, these values differ considerably due to the so-called "memory effect". Even so the memory or influence of higher layers on the effective layer optical depth is much less than the effect of absorber amount and temperature within the layer.

The following terms for the regression of K_i were considered:

Symbol	Units	Description
ΔU_i	g/cm^2	Integrated H_2O layer amount
ΔT_i	°K	Layer mean temperature difference from standard temperature.
$\Delta U_i \Delta T_i$	$(g°K)/cm^2$	Temperature weighted layer H_2O amount

Symbol	Units	Description
U_i	g/cm^2	Total H_2O from top of atmosphere to level i.
$T_i^* = \int_0^{P_i} PT\frac{\partial U}{\partial P}\partial P$	$°Kmb.g/cm^2$	H_2O - pressure - temperature

The least squares solution for K_i could thus be expressed:

$$K_i = a\Delta U_i + b\Delta U_i\Delta T_i + cU_i + d\Delta T_i + e\,T_i^* + f \qquad \text{(A3)}$$

where the constants a-f are to be determined by a least squares regression procedure for each level and every channel. The term f is a constant factor that serves to reduce any bias in the procedure.

Preliminary tests run with several of the SSH/2 channels made clear that all of the suggested terms were significant in most cases except the term ΔT_i. Significance was determined by using an f test to calculate $P(H_o)$, the probability that the regression coefficient equals zero. The reason the term ΔT_i did not pass this test, while the combination term $\Delta T_i\Delta U_i$ did pass, is that channels 7-14 of the SSH/2 have almost all of their absorption by H_2O. Variations in temperature with small amounts of water vapor present would have a small effect, while variations in temperature at high humidities would have a large effect.

The terms T* and U_i are included to account for the "memory" effect on the atmosphere and were found significant in most cases. The top several layers of the atmosphere consistently gave bad fits. This was felt to be a result of the relatively small amount

of absorption above 50 mb. For these layers a simple two term regression was used

$$K_i = a\ \Delta U_i + b \tag{A4}$$

One further change was made to the regression model (B3). There is a physical reason to believe that the dependence of optical depth is not always a linear function of absorber amount. Theory predicts a variation of $K \sim U^{\gamma}$ where $\gamma = 1$ in the case of weak absorption (the "weak line limit") and $\gamma = .5$ in the case of strong absorption (the "strong line limit"). The terms ΔU_i, $\Delta U_i \Delta T_i$ and U_i were replaced by $\Delta U_i^{\gamma 1}$, $\Delta U_i^{\gamma 2}.\Delta T_i$, and $U^{\gamma 3}{}_i$. To simplify matters we chose $\gamma 1 = \gamma 2 = \gamma 3 = \gamma$ and the gammas were selected by an iterative procedure that optimized the percent variance explained by the regression model. The variations in the gammas were restricted to steps of .1. A more sophisticated procedure would allow the selection of different gammas, and would not restrict them to integral multiples of .1. Future versions of the rapid algorithm may include these enhancements.

4. Generation and Testing of the Rapid Algorithm Coefficients

The final model selected for the rapid algorithm is,

$$K_i = a\Delta U_i^{\gamma} + b\Delta u_i^{\gamma}\Delta T_i + CU_i^{\gamma} + dT_i^{*} + e \tag{A5}$$

and the transmittances $\tau(P_I)$ are constructed as follows,

$$T(P_I) = \exp\ (-\sum_{i=1}^{I} K_i) \tag{A6}$$

Coefficients were generated for the eight water vapor channels 7-14 for the 24 level coordinate system described in Section 4.4.

The most important test of the rapid algorithm is the accuracy of the brightness temperatures (T_B) and radiances (r) generated with it. A comparison was made between r and T_B generated by the rapid algorithm and the exact method; the results are shown in Table A1 for both the dependent and independent data sets along with the noise equivalent ΔT_B of the SSH/2.

The mean error of T_B and r gives the bias. The root-mean-square error is a measure of the absolute size of the error without the bias removed. A subsequent correction for bias in T_B and r values can reduce this error further. As expected, the errors are smaller in the dependent data set than in the independent data set. The bias of most channels is less than the rms error but is still probably worth correcting.

The most critical comparison is between the instrument noise equivalent ΔT_B ($NE\Delta T_B$) and the independent data set rms error. For most channels these two quantities are comparable. These results are shown in Table A1. Some problems were encountered with channels 12 and 13, however, where the errors were somewhat greater than twice the $NE\Delta T_B$.

The instrument induced noise is generally much less than the so-called "atmospheric" noise: errors introduced by inexact correction for clouds in the field of view, uncertainties in the line parameters, the water vapor continuum assorption, and problems with the radiative transfer equation.

CHANNEL NUMBER (CODE)	MEAN ERROR T_B (°K)		RMS ERROR T_B (°K)		INSTRUMENT NOISE EQUIVALENT ΔT_B (°K)
	independent	dependent	independent	dependent	
7 (E7)	-0.04	0.00	0.05	0.07	0.03
8 (F1)	0.04	0.01	0.06	0.02	0.12
9 (F5)	0.04	0.01	0.08	0.03	0.12
10 (F6)	0.04	0.00	0.15	0.03	0.14
11 (F4)	0.02	0.00	0.12	0.03	0.06
12 (F3)	0.03	0.00	0.26	0.05	0.11
13 (F2)	-0.05	-0.01	0.35	0.07	0.19
14 (F8)	-0.11	-0.01	0.36	0.07	0.47

CHANNEL NUMBER	MEAN ERROR IN RADIANCE, (%)		RMS ERROR IN RADIANCE, (%)	
	independent	dependent	independent	dependent
7 (E7)	-0.07	-0.01	0.10	0.12
8 (F1)	0.07	0.01	0.10	0.03
9 (F5)	0.07	0.02	0.13	0.04
10 (F6)	0.06	0.00	0.26	0.05
11 (F4)	0.03	0.01	0.21	0.04
12 (F3)	0.05	-0.01	0.46	0.08
13 (F2)	-0.10	-0.02	0.63	0.13
14 (F8)	-0.20	-0.03	0.67	0.13

Table A-1 Errors in Calculated Brightness Temperatures Caused by Using the Rapid Transmittance Algorithm for Dependent and Independent Sets

The wide range of profiles in the independent data set provided a stringent test of the rapid algorithm. The range in total integrated water vapor amount from the driest to wettest profile spanned two orders of magnitude. This relatively simple algorithm performed quite well over this extreme variation.

5. Summary

An adequate rapid algorithm for the purposes of this study has been developed and tested. Since transmittances and radiances generated from the rapid algorithm will be considered as truth for the first guess retrieval and relaxation procedure, it is only required that the behavior of the rapid algorithm with temperature and moisture variations approximates that of the exact procedure; this has been demonstrated by the independent data test.

APPENDIX B

REFERENCES

APPENDIX B: References

1. Smith, W.L., and H.M. Woolf, 1976.
   The use of eigenvectors of statistical covariance matrices for interpreting satellite sounding radiometer observations.
   J. Atmos. Sci., 33, 1127-1140.

2. Chahine, M.T., 1970.
   Inversion problems in radiative transfer: determination of atmospheric parameters.
   J. Atmos. Sci., 27, 960 967.

3. King, J.I.F., 1963.
   Meteorological Inferences from Satellite Radiometry I.
   J. Atmos. Sci., 20, 245-250.

4. Kaplan, L.D. 1959.
   Inference of atmospheric structure from remote radiation measurements.
   J. Opt. Soc. Amer., 49, 1004-1007.

5. Wark, D.Q. and H.E. Fleming, 1966.
   Indirect measurements of atmospheric temperatures from satellites.
   Mon. Wea. Rev., 351.

6. Barnes Engineering Company, 1978.
   Special Sensor H-2 (SSH-2) Total System Spectral Response S/N 006-008.
   Air Force Contract F04701 76-C-0058, Item 0001AE.

7. Susskind, J. et al., 1977
GISS VTPR Processing Manual
NASA, Goddard Space Flight Center, Greenbelt, Maryland, January 1977.

8. Rothman, L.S., 1980.
AFGL atmospheric absorption line parameters compilation: 1980 version.
Applied Optics, 20, 791.

9. McClatchey, R.A. et al., 1972.
Optical Properties of the Atmosphere
AFCRL-72-0497, Air Force Cambridge Research Laboratories, Bedford, MA, August, 1972.

10. Twomey, S. 1977.
Introduction to the Mathematics of Inversion in Remote Sensing and Indirect Measurements.
Elsevier, New York

11. Householder, A.S., 1964.
The Theory of Matrices in Numerical Analysis.
Blaisdell Publishing Co., New York.

12. Smith, W.L., and H.B. Howell, 1971.
Vertical distribution of atmospheric water vapor from satellite infrared spectrometer measurements.
J. Appl. Meteor., 10, 1026-1034.

DISTRIBUTION: CR 83-01(a),(b) [VOLUMES 1, 2]

SPECIAL ASST. TO THE ASST. SECNAV (R&D)
RM 4E741, THE PENTAGON
WASHINGTON, DC 20350

CHIEF OF NAVAL RESEARCH
LIBRARY SERVICES, CODE 734
RM 633, BALLSTON TOWER #1
800 QUINCY ST.
ARLINGTON, VA 22217

OFFICE OF NAVAL RESEARCH
ATTN: DR. REED, CODE 100B1
ARLINGTON, VA 22217

OFFICE OF NAVAL RESEARCH
CODE 422AT
ARLINGTON, VA 22217

OFFICE OF NAVAL RESEARCH
CODE 420
ARLINGTON, VA 22217

OFFICE OF NAVAL RESEARCH
COASTAL SCIENCES PROGRAM
CODE 422 CS
ARLINGTON, VA 22217

CHIEF OF NAVAL OPERATIONS
(OP-952)
U.S. NAVAL OBSERVATORY
WASHINGTON, DC 20390

CHIEF OF NAVAL OPERATIONS
NAVY DEPT. OP-986G
WASHINGTON, DC 20350

CHIEF OF NAVAL OPERATIONS
U.S. NAVAL OBSERVATORY
DR. R. JAMES, OP-952D1
34TH & MASS. AVE., NW
WASHINGTON, DC 20390

CHIEF OF NAVAL MATERIAL
NAVY DEPT., MAT-0724
WASHINGTON, DC 22332

NAVAL DEPUTY TO THE ADMINISTRATOR, NOAA
RM. 200, PAGE BLDG. #1
3300 WHITEHAVEN ST., NW
WASHINGTON, DC 20235

OFFICE OF STAFF METEORO.
WESTERN SPACE & MISSILE CENTER (WE)
VANDENBERG AFB, CA 93437

OFFICE OF NAVAL RESEARCH
E. CENTRAL REGIONAL OFFICE
BLDG. 114, SECT. D
459 SUMMER ST.
BOSTON, MA 02210

COMMANDING OFFICER
OFFICE OF NAVAL RESEARCH
1030 E. GREEN ST.
PASADENA, CA 91101

OFFICE OF NAVAL RESEARCH
SCRIPPS INSTITUTION OF OCEANOGRAPHY
LA JOLLA, CA 92037

COMMANDING OFFICER
NORDA, CODE 335
NSTL STATION
BAY ST. LOUIS, MS 39529

COMNAVOCEANCOM
NSTL STATION
BAY ST. LOUIS, MS 39529

COMMANDING OFFICER
NAVOCEANO LIBRARY
NSTL STATION
BAY ST. LOUIS, MS 39522

COMMANDING OFFICER
FLENUMOCEANCEN
MONTEREY, CA 93940

COMMANDING OFFICER
NAVPOLAROCEANCEN
NAVY DEPT.
4301 SUITLAND RD.
WASHINGTON, DC 20390

COMMANDER
NAVAIRSYSCOM
ATTN: LIBRARY, AIR-00D4

COMMANDER
NAVAIRSYSCOM (AIR-333)
WASHINGTON, DC 20361

COMMANDER
NAVAIRSYSCOM (AIR-553)
WASHINGTON, DC 20360

NATIONAL SCI. FOUNDATION
HEAD, ATMOS. SCI. DIV.
1800 G STREET, NW
WASHINGTON, DC 20550

COMMANDER
NAVOCEANSYSCEN
DR. J. RICHTER, CODE 532
SAN DIEGO, CA 92152

COMMANDER
NAVAL SURFACE WEAPONS CENTER
DR. B. KATZ, WHITE OAKS LAB
SILVER SPRING, MD 20910

COMMANDER
NAVAL SURFACE WEAPONS CENTER
ATTN: CODE 44
DAHLGREN, VA 22448

NAVAL SPACE SYSTEMS ACTIVITY, CODE 60
P.O. BOX 92960
WORLDWAY POSTAL CENTER
LOS ANGELES, CA 90009

NAVAL POSTGRADUATE SCHOOL
METEOROLOGY DEPT., CODE 63
MONTEREY, CA 93940

NAVAL POSTGRADUATE SCHOOL
OCEANOGRAPHY DEPT., CODE 68
MONTEREY, CA 93940

NAVPGSCOL
LIBRARY, CODE 0142
MONTEREY, CA 93940

COMMANDER
AWS/DN
SCOTT AFB, IL 62225

SUPERINTENDENT
ATTN: USAFA(DEG)
USAF ACADEMY, CO 80840

AFGWC/DAPL
OFFUTT AFB, NE 68113

3 WW/DN
OFFUTT AFB, NE 68113

AFGL/LY
HANSCOM AFB, MA 01731

AFGL/OPI
HANSCOM AFB, MA 01731

OREGON STATE UNIVERSITY
ATMOS. SCIENCES DEPT.
CORVALLIS, OR 97331

AFOSR/NC
BOLLING AFB
WASHINGTON, DC 20312

COMMANDER & DIRECTOR
ATTN: DELAS-DM-A
U.S. ARMY ATMOS. SCI. LAB
WHITE SANDS MISSILE RANGE
WHITE SANDS, NM 88002

COMMANDING OFFICER
U.S. ARMY RESEARCH OFFICE
ATTN: GEOPHYSICS DIV.
P.O BOX 12211, RESEARCH
TRIANGLE PARK, NC 27709

DIRECTOR
DEFENSE TECHNICAL INFORMATION
CENTER, CAMERON STATION
ALEXANDRIA, VA 22314

DIRECTOR
NATIONAL METEOROLOGICAL
CENTER, NWS, NOAA
WWB W32, RM 204
WASHINGTON, DC 20233

DIRECTOR, NATIONAL EARTH
SATELLITE/SEL
FB-4, S321B
SUITLAND, MD 20233

FEDERAL COORDINATOR FOR
METEOROLOGICAL SERVICES
& SUPPORT RSCH. (OFCM)
11426 ROCKVILLE PIKE
SUITE 300
ROCKVILLE, MD 20852

CHIEF, MESOSCALE
APPLICATIONS BRANCH
NATIONAL EARTH SAT. SERV.
1225 W. DAYTON
MADISON, WI 53562

DIRECTOR
TECHNIQUES DEVELOPMENT LAB
GRAMAX BLDG.
8060 13TH ST.
SILVER SPRING, MD 20910

LABORATORY FOR ATMOS.
SCIENCES, NASA
GODDARD SPACE FLIGHT CEN.
GREENBELT, MD 20771

EXECUTIVE SECRETARY, CAO
SUBCOMM. ON ATMOS. SCI.
NATIONAL SCI. FOUNDATION
RM 510, 1800 G. ST., NW
WASHINGTON, DC 20550

UCLA
ATMOSPHERIC SCIENCES DEPT.
405 HILGARD AVE.
LOS ANGELES, CA 90024

NATIONAL CENTER FOR ATMOS.
RSCH., LIBRARY ACQUIS.
P.O. BOX 3000
BOULDER, CO 80302

COLORADO STATE UNIVERSITY
ATMOS. SCI. DEPT.
ATTN: DR. R. PIELKE
FT. COLLINS, CO 80523

DIRECTOR, REMOTE SENSING
LAB, UNIV. OF MIAMI
P.O. BOX 248003
CORAL GABLES, FL 33124

DIRECTOR
COASTAL STUDIES INSTITUTE
LOUISIANA STATE UNIV.
ATTN: O. HUH
BATON ROUGE, LA 70803

JOHNS HOPKINS UNIVERSITY
APPLIED PHYSICS LAB
R.E. GIBSON LIBRARY
JOHNS HOPKINS ROAD
LAUREL, MD 20810

CHAIRMAN
METEOROLOGY DEPT.
MASSACHUSETTS INSTITUTE
OF TECHNOLOGY
CAMBRIDGE, MA 02139

TEXAS A&M UNIVERSITY
METEOROLOGY DEPT.
COLLEGE STATION, TX 77843

UNIVERSITY OF WASHINGTON
ATMOS. SCIENCES DEPT.
SEATTLE, WA 98195

CHAIRMAN, METEORO. DEPT.
UNIVERSITY OF WISCONSIN
1225 W. DAYTON ST.
MADISON, WI 53706

COLORADO STATE UNIVERSITY
ATMOS. SCI. DEPT.
ATTN: LIBRARIAN
FT. COLLINS, CO 80523

CONTROL DATA CORP.
METEOROLOGY, RSCH. DIV.
2800 E. OLD SHAKOPEE RD.
BOX 1249
MINNEAPOLIS, MN 55440

AEROSPACE CORPORATION
METEOROLOGY SECTION
P.O. BOX 92957
LOS ANGELES, CA 90009

OCEAN DATA SYSTEMS, INC.
2460 GARDEN ROAD
MONTEREY, CA 93940

SYS. & APPLIED SCI. CORP.
ATTN: LIBRARY, SUITE 500
6811 KENILWORTH AVE.
RIVERDALE, MD 20840

RCA GOVERNMENT SYS. DIV.
ASTRO-ELECTRONICS
ATTN: A. ROSENBERG
PRINCETON, NJ 08540

THE EXECUTIVE DIRECTOR
AMERICAN METEORO. SOCIETY
45 BEACON ST.
BOSTON, MA 02108

AMERICAN METEORO. SOCIETY
METEO./GEOASTRO ABSTRACTS
P.O. BOX 1736
WASHINGTON, DC 20013

CAPT W.G. SCHRAMM (USN/RET)
C/O NCOIC
MARINE SECURITY GUARD DET.
US MISSION, GENEVA
DEPT. OF STATE
WASHINGTON, DC 20520

DR. HENRY FLEMING
NOAA/NESS S321-B
FEDERAL BLDG. #4
SUITLAND, MD 20023

M. T. CHAHINE
JET PROPULSION LAB
4800 OAK GROVE DR.
PASADENA, CA 91109

R. HASKINS
JET PROPULSION LAB
4800 OAK GROVE DR.
PASADENA, CA 91109

JAPAN METEORO. AGENCY
3-4 OTEMACHI 1-CHOME,
CHIYODA-KU
TOKYO 100, JAPAN

D. J. MCCLEESE
JET PROPULSION LAB
4800 OAK GROVE DR.
PASADENA, CA 91109

JOEL SUSSKIND
CODE 911
GODDARD SPACE FLIGHT CEN.
GREENBELT, MD 20771

LIBRARY
CSIRO DIV. ATMOS. PHYS.
STATION STREET
ASPENDALE, 3195
VICTORIA, AUSTRALIA

BUREAU OF METEOROLOGY
ATTN: LIBRARY
BOX 1289K, GPO
MELBOURNE, VIC, 3001
AUSTRALIA

LIBRARY
AUSTRALIAN NUMERICAL
METEO. RSCH. CENTER
P.O. BOX 5089A
MELBOURNE, VICTORIA, 3001
AUSTRALIA

LIBRARY
ATMOS. ENVIRONMENT SERV.
4905 DUFFERIN ST.
DOWNSVIEW M3H 5T4
ONTARIO, CANADA

BIBLIOTECA
INSTITUTE ANARTICO CHILENO
LUIS THAYER OJEDA 814
SANTIAGO, CHILE

METEORO. OFFICE LIBRARY
LONDON ROAD
BRACKNELL, BERKSHIRE
RG 12 1SZ, ENGLAND

EUROPEAN CENTRE FOR MEDIUM
RANGE WEATHER FORECASTS
SHINFIELD PARK, READING
BERKSHIRE RG29AX, ENGLAND

HEAD, DATA PROCESSING SEC.
GERMAN MILITARY GEOPHYS.
MOUT-ROYAL, D-5580
TRAVEN-TRARBACH
FEDERAL REPUBLIC OF GERMANY